Palynological and organic geochemical characterization of marine and terrestrial Early Pleistocene climate in northwest Europe

This thesis is submitted to Utrecht University in accordance with the requirements to obtain the degree Master of Science in Biogeology

N.A.G.M. van Helmond

Supervision:

Dr. J.W.H. Weijers (UU) & Dr. T.H. Donders (TNO)

Affiliated staff member:

Dr. G.J. Reichart (UU)

August 2010

Table of contents

Abstract

Ever since the Eocene Thermal Maximum, ~52-50 Ma, Cenozoic long-term climate evolution is characterized by a global cooling trend. In the Northern Hemisphere, this development eventually let to large scale glaciations from the Pliocene-Pleistocene transition (~2.6 Ma) onward. The exact rate and characteristics of this key transition on both land and sea in the Northern Hemisphere is yet unclear.

Two marine cores, A15-3 and A15-4, from the northwestern part of the Dutch North Sea basin contain extensive Eridanos river delta sediments covering this transition. Paleomagnetic data, dinocyst and pollen records and foraminiferal proxies have provided a solid integrated timeframe. Gamma ray and magnetic susceptibility logs show presumed obliquity-length cycles, expressed in alternating clay and coarser grained sand layers, that were tentatively correlated with Marine Isotope Stages 103 to 94. Therefore, these cores are well suited for a high resolution coupled climate reconstruction of the terrestrial and marine environments during the Early Pleistocene. This climate reconstruction was obtained by generation of high resolution pollen records and records of several (organic) geochemical proxies. The main focus of this thesis lies on the application of novel paleotemperature proxies based on the distribution of glycerol dialkyl glycerol tetraethers, membrane lipids produced by microorganisms.

Petrochemical proxies based on the distribution of long chain *n*-alkanes in combination with the C/N ratio and the Branched vs. Isoprenoid Tetraether (BIT) index generally show a dominant terrestrial derived source for the organic matter in the studied sediments, although there are episodes with increased marine influence coupled to sea level variations. High resolution pollen records and dinocyst assemblage scans show a dominance of “warm taxa”, e.g. *Osmunda* spores and *Operculodinium israelianum* cysts, in the coarser grained intervals. The clay intervals, on the contrary, are dominated by “cool taxa”, e.g. Ericaceae pollen and *Filisphaera* cysts. The organic geochemical paleothermometers TEX_{86} and MBT/CBT, used for the reconstruction of sea surface temperatures (SSTs) and annual mean air temperatures (MATs), respectively, show high temperatures in the clay intervals, with SSTs up to ~17°C and MATs up to ~21°C. For the coarser intervals lower temperatures are reconstructed, with SST minima close to 9°C and MAT minima around 6.5°C. Amplitudes in temperature reconstructions are comparable with results of previous studies, absolute temperatures are higher than expected. The organic geochemical proxies contradict the palynology, and thus the

previously established tentative correlation to the Marine Isotope Stages. A possible explanation for the difference in phasing between palynology and the organic geochemical proxies is found in the two different source areas were the deposited sediments are transported from, in combination with reworking by deltaic and fluvial dynamics.

The different marine and terrestrial climate proxies are generally in phase with each other, from which it is concluded that there was a strong climate coupling of marine and terrestrial environments in the Early Pleistocene of northwest Europe.

1. Introduction

1.1 Cenozoic climate evolution

The Cenozoic Era (*appendix 1*) is the most recent of the three classic geological eras (Paleozoic, Mesozoic, Cenozoic) and covers the period from 65.5 million years ago (Ma) to present. During early Cenozoic times our planet is commonly characterized as a 'Greenhouse World' (*fig.1*), with no ice and high temperatures (e.g., Zachos et al., 2001; Pearson et al., 2007). At certain moments in the early Cenozoic, temperatures in the polar regions even reached subtropical values like during the Paleocene Eocene Thermal Maximum (PETM), ~55.8 Ma (Sluijs et al., 2006; Weijers et al., 2007) and at the Eocene Thermal Maximum 2 (ETM2), ~52-50 Ma. Since ETM2, Cenozoic climate is characterized by a global cooling trend (e.g. Flower and Kennett,1994; Zachos et al., 2001; Holbourn et al., 2005; Zachos et al., 2008).

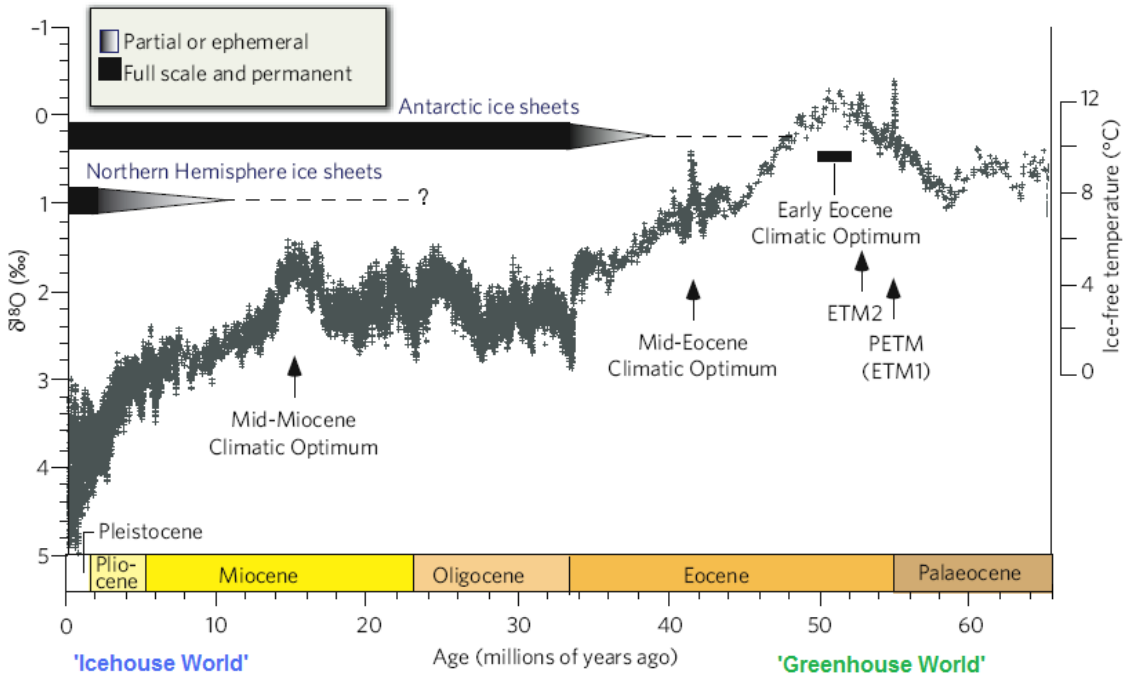

Figure 1) Cenozoic climate evolution based on stacked deep-sea benthic foraminiferal oxygen-isotope records (Zachos et al., 2008).

The widespread occurrence of large glaciations started on Antarctica ~34 Ma. A shift towards lower temperatures, caused by long-term CO_2 decrease (DeConto and Pollard,

2003), at the Eocene/Oligocene boundary, studied for the Northern Hemisphere by Schouten et al. (2008), is associated with this first large icecap formation (Zachos et al. 1996; Barrett, 1996, Lear et al., 2000; Zachos et al., 2001).

During the Oligocene and Miocene, cooling of our planet continued. The climate evolution of the Miocene in NW Europe was studied in high resolution by Donders et al. (2009a), who showed a cooling trend in both the marine and terrestrial realms based on both palynological and organic geochemical records. Quantitative reconstruction of annual mean air temperature based on the distribution of fossil branched glycerol dialkyl glycerol tetraethers, showed a cooling from ~27°C to ~14°C between 17 and 5 Ma punctuated by short-term variations.

The Pliocene-Pleistocene transition (2.588 Ma) is a key period of the Cenozoic climate development, since the frequency, amplitude and extension of Northern Hemisphere glaciations (Lisiecki and Raymo, 2005; *fig.2*) increased dramatically around this boundary (Clark et al., 1999). Many theories have been put forward to explain the initiation of these glaciations, e.g. tectonic explanations (Hay, 1992; Raymo, 1994), orbital forcing (Maslin et al. 1998) and a recent study (Etourneau et al., 2010) assumes that the intensification of atmospheric circulation in the tropics and subtropics significantly contributed to the initiation of continental ice sheet formation at high latitudes around the Pliocene-Pleistocene transition. The considerable change in climate regime had severe impacts on flora and fauna, resulting in several regional extinctions among groups of flora (Svenning, 2003), already reported by Zagwijn (1974b). Also mammals were impacted by the transition to the glacial-interglacial cycles, for instance, a severe decrease in Soricinae (shrews) diversity was reported by Reumer (1989).

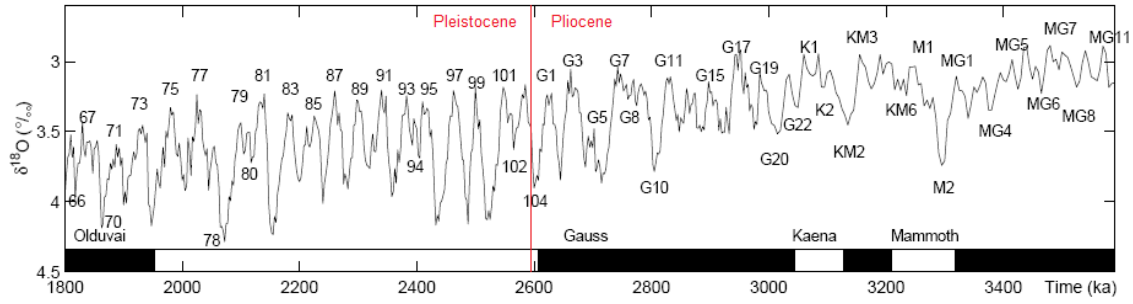

Figure 2) The intensification of the Northern Hemisphere glaciations is visible in stacked deep-sea benthic foraminiferal oxygen-isotope records. Numbers in the Pleistocene part of the figure indicate Marine Isotope Stages. Figure adapted from Lisiecki and Raymo (2005).

Bintanja and Van de Wal (2008) used the stacked deep-sea benthic foraminiferal oxygen-isotope records of Lisiecki and Raymo (2005) as input for a model to reconstruct surface air temperatures for North America over the last three million years. Although the study of Bintanja and Van de Wal (2008) comprises the Pliocene-Pleistocene transition, a high resolution multi proxy study is needed for a better understanding of the climate evolution around this important transition.

This study combines both palynological and (novel) organic geochemical proxies. The aim of this study is to determine the exact phase relation between the marine and terrestrial climate shift, and the rate and degree of cooling in a detailed Milankovitch-scale resolution during the Early Pleistocene in NW Europe. In combination with detailed isotopic data and recent new paleoatmospheric CO_2 data (Seki et al., 2010) the results of this study can provide an integrated view of Early Pleistocene climate conditions, which can be used to validate climate models (e.g. Huber and Sloan, 2001).

1.2 Previous work

The current work proceeds the work by Kuhlmann (2004) and several internal reports from the Geological Survey of the Netherlands (e.g. Donders et al., 2009b). The earlier research focused on high resolution stratigraphy and paleoenvironmental changes in the southern North Sea during the Neogene, gathering information on the paleoenvironments. A combination of dinoflagellate records, pollen records, isotopic data, gamma ray and magnetic susceptibility logs, mainly originating from two exploration wells A15-3 and A15-4, showed an onset of severe cold periods around the Pliocene-Pleistocene transition. Gamma ray and magnetic susceptibility logs show obliquity cycles that correlate with Marine Isotope Stages (MIS) 103 to 94 for this period (fig. 3). A recent MSc thesis from Welkenhuysen (Katholieke Universiteit Leuven, 2006) provides information on the benthic foraminiferal assemblages to which the pollen and isotopic data can be compared. Notwithstanding the importance of this previous work, a true high resolution multi-proxy study has not been performed yet. Therefore, this new study combines palynological records in high resolution with new organic geochemical proxies (e.g. delivering absolute temperature estimates). Together, these proxies will provide detailed insights in the climate evolution around this important transition, comprising MIS 103 to 94.

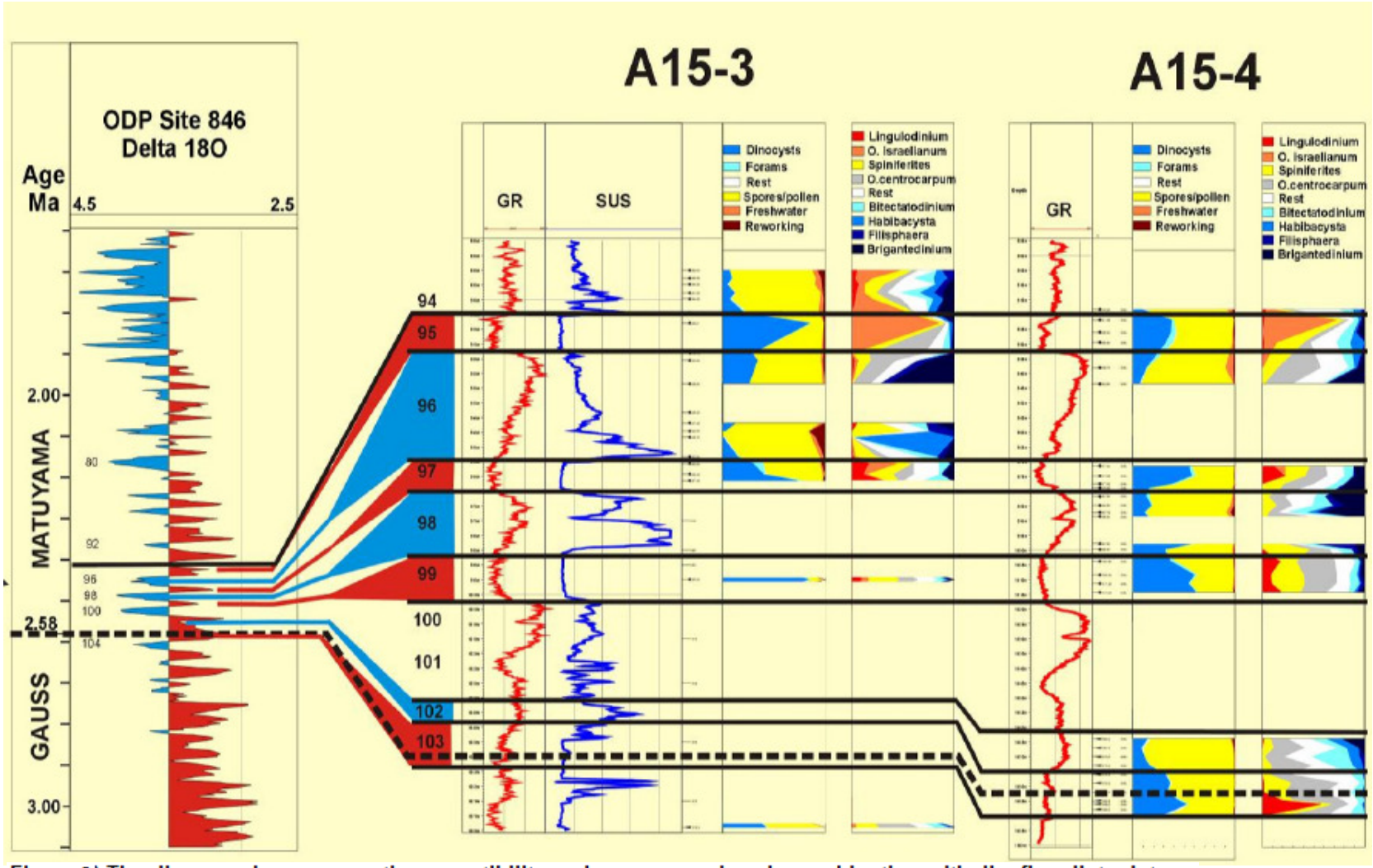

Figure 3) The diagram shows magnetic susceptibility and gamma ray logs in combination with dinoflagellate data for cores A15-03 and A15-04. Furthermore oxygen isotope information is added coupled to the marine isotope stages.

1.3 Proxies used for climate reconstruction

1.3.1 Palynology

Pollen and spores records are a reliable source to reconstruct terrestrial paleoenvironments and paleoclimate (Birks and Birks, 1980). Although pollen assemblages are very sensitive to changes in climate and environment, it is important to be aware of some problems that might occur. Terrestrial records, including pollen records, are often associated with chronostratigraphical problems, high spatial variability, and discontinuous accumulation (Pross and Klotz, 2002; Kemna and Westerhoff, 2007; Donders et al., 2007). As this study makes use of shallow marine sediments, problems associated to these continental-based records are not having a large influence. Still, problems remain concerning differential transport of pollen by water or wind. Differential transport can bias the pollen assemblages. Assemblages with a relatively high number of taxa, including insect pollinated forms, are indicative of substantial pollen input through water transport (Whitehead, 1983), whereas wind-transported pollen typically show a low-diversity (Hooghiemstra, 1988). Sediments of a location proximal to a river delta likely receive a majority of pollen that are water-transported. On the other hand, sediments from more distal locations are dominated by wind-transported pollen. Together, this means that it has to be taken into account that glacial-interglacial cycles, with related sea-level-changes and varying fluvial input, will influence the pollen deposition and assemblage composition through time.

Pollen records are based on relative occurrences of species within an assemblage. Interglacial periods are associated with relatively warmer and wetter climatic conditions on the continent. These periods are usually marked by (increased) occurrences of thermophilous trees (like *Acer, Carpinus, Carya, Corylus, Fagus, Ilex, Ostrya, Olea, Tilia, Ulmus*, *Quercus, Alnus, Fraxinus, Myrica* and *Pterocarya*), swamp vegetation (e.g., *Taxodium, Sequoia, Cupressaceae, Sciadopitys, Eucommia, Liquidambar, Elaegnus, Nyssa, Rhus* and *Symplocos*), conifers like *Picea and Tsuga,* and ferns like *Osmunda*. Another often appearing fern is *Dryopteris*. Appearances of *Dryopteris* are quite random. During glacial periods terrestrial climate is characterized by cooler and dryer conditions. Glacials are marked by (increased) occurrences of heath vegetation (e.g. *Ericaceae*) and herbs (e.g. *Sphagnum*). Real extensive polar climate allows hardly any vegetation to

grow (e.g. polar dessert). These periods are characterized by low pollen counts. *Pinus* abundance is strongly related to the relative distance to the coast, and hence can be influenced by sea-level changes.

A combination of pollen records with records of dinoflagellate cysts, which typically occur under neritic conditions, enables synchronous reconstruction of marine and terrestrial paleoenvironments (Donders et al., 2009a). Dinoflagellate cysts (dinocysts) records are also based on relative occurrences. Species–environment relations can be empirically deduced from comparisons with other fossil groups (e.g. foraminifera) or physical and chemical evidence, as well as by comparing distributions of extinct taxa with species for which the ecology is better known (Versteegh and Zonneveld, 1994; Sluijs et al., 2005). Relative sea surface temperature (SST) and different inshore to offshore water mass conditions (e.g. Brinkhuis, 1994; Versteegh and Zonneveld, 1994) can be deduced from pre-Quaternary dinocyst assemblages (e.g. see Sluijs et al., 2005; Pross and Brinkhuis, 2005). Water mass conditions, in turn, depend on sea-level variations, which can thus be detected using relative changes in the dinocyst assemblages (Donders et al., 2009a). Interglacial periods are associated with relative warm seawater temperatures, for both surface and deep waters. During warmer stages salinity is usually lower (less water stored in icecaps and increased runoff) and productivity is higher because of high amounts of nutrients. This is predominantly expressed by increased occurrences of the dinocysts *Lingulodinium machaerophorum* and *Operculodinium israelianum* (Kuhlmann, 2004). Furthermore a large diversity of dinocysts can be associated with these circumstances (e.g. *Barssidinium* spp., *Impagidinium aculeatum*, *Impagidinium multiplexum*, *Operculodinium eirikianum*, *Tuberculodinium vancampoae*, *Tectatodinium pellitum*). During glacials, seawater is cooler and runoff and productivity are relatively low. These periods are characterized by occurrences of the heterotrophic *Brigantedinium* spp. and enhanced occurrences of the *Habibacysta*/*Filisphaera group* and *Bitectatodinium tepikiense*. Occurrences of widely occurring *Spiniferites spp.* and *Operculodinium centrocarpum* are more complicated to interpret, due to their widespread occurrence (Marret and Zonneveld et al., 2003).

1.3.2 Organic geochemistry

Total Organic Carbon (TOC) content provides information on the amount of organic carbon present in sediments relative to the mineral fraction. Together with total nitrogen measurements the atomic C/N ratio can be calculated. Because this ratio in seawater is more or less constant (value), i.e. determined by the Redfield ratio (Redfield, 1934), marine organic matter will show C/N values close to this value. Since C/N ratios of terrestrial organic matter are much higher, the C/N ratios of organic matter in near coastal marine sediments can give an indication of the preferential source, i.e. marine or terrestrial.

Many microorganisms leave traces behind in sedimentary records in the form of fossilized chemical components. If these components are specific to a certain organism or a group of organisms, these molecules are referred to as biomarkers. In addition to being specific for an organism, these molecular fossils might also provide information on the paleoenvironment and paleoclimate where the organism lived in.
Saturated hydrocarbons, termed *n*-alkanes, are important constituents in different groups of organisms. Marine organisms typically contain short chain (C_{16}-C_{24}) *n*-alkanes, whereas the leaf waxes of land plants dominantly contain long chain (C_{25}-C_{35}) *n*-alkanes. Leaf wax-derived lipids from grasses, on average, contain *n*-alkanes with longer chain lengths (C_{31}-C_{33}) than those from higher plants (Cranwell, 1973). Peat mosses like Sphagnum, on the other hand, are characterized by a dominance of the shorter C_{23} *n*-alkane (Nichols et al., 2006). The long chain (C_{25}–C_{35}) *n*-alkane distribution of vascular land plants exhibits high odd-over-even predominance. A common petrochemical proxy derived from this predominance is the Carbon Preference Index (CPI). CPI is calculated for the *n*-alkanes C_{25}-C_{33}, and is an indicator for the source of these *n*-alkanes. Hydrocarbons composed of a mixture of compounds originating from terrestrial plant material show CPI values ranging between ~5-10 (Rieley et al., 1991; Hedges and Prahl, 1993). CPI values close to one are thought to indicate greater input from marine microorganisms and/or recycled organic matter (Kennicutt et al., 1987). Another often used petrochemical proxy is based on the average chain length of *n*-alkanes (ACL). ACL describes the average number of carbon atoms per molecule based on the abundance of the odd-carbon-numbered higher plant n-alkanes (Poynter and Eglinton, 1990) and is calculated for the *n*-alkanes C_{27}-C_{33}. ACL is mainly determined by the type

of vegetation and is, therefore, used as a measure for the hydrocarbon source and to determine the consistence of the organic matter input in proximal basins Jeng (2006) made a comparison between ACL for river sediments and marine sediments around Taiwan. For river sediments ACL ranged from 29.2 to 30.5 and for marine sediments from 28.4 to 29.3.

Long chain alkenones (*fig.4*), compounds synthesised by haptophyte algae, can provide an additional means to reconstruct SST by means of the UK'_{37} index (Prahl and Wakeham, 1987; Müller et al.1998). The UK'_{37} proxy is based on the fact that the degree of unsaturation in alkenones depends on the temperature of the water where alkenone producing organisms thrive. Haptophyte algae living in warm water will produce relatively more alkenones with a low degree of unsaturation (C37:2), while haptophyte algae living in colder water will produce relatively more alkenones with a higher degree of unsaturation (C37:3, *fig.4*).

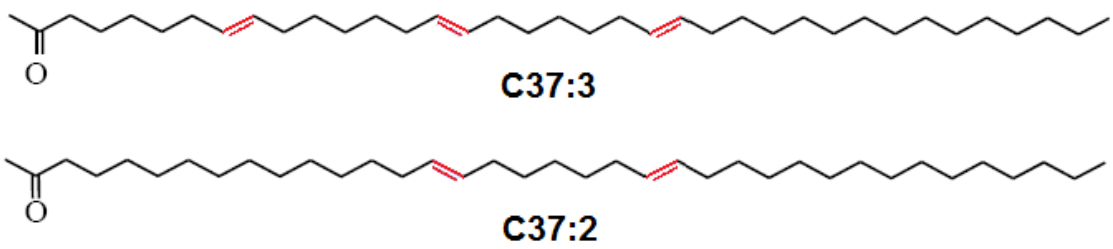

Figure 4) Chemical structures of the long chain alkenones, used in the calculation of the UK'_{37} index. The differences in the degree of unsaturation are indicated in red.

A relatively novel group of biomarkers are the glycerol dialkyl glycerol tetraethers (GDGTs), which are core membrane lipids synthesized mainly by archaea and some bacteria. GDGTs are divided in two groups: branched GDGTs and isoprenoid GDGTs (*fig.5*). Branched GDGT membrane lipids are thought to be derived from anaerobic soil bacteria (Weijers et al., 2006a,b) and isoprenoid GDGT membrane lipids are mainly derived from marine pelagic Crenarchaeota (e.g. Schouten et al., 2000). GDGTs are used in several novel proxies used for climate reconstructions.

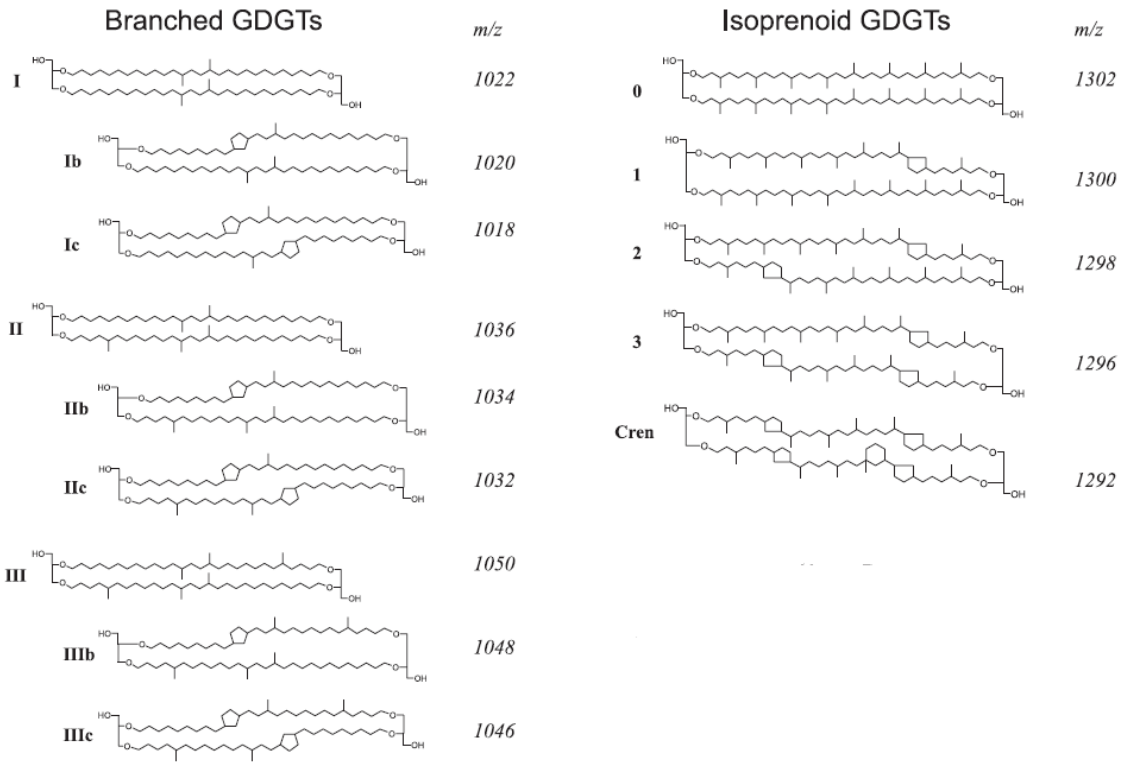

Figure 5) Chemical structures of the branched GDGTs, used in the calculation of MBT and CBT, and isoprenoid GDGTs, used for the calculation of the TEX_{86} index. Cren = Crenarcheol. (Weijers, 2007)

The TEtraether indeX of isoprenoid GDGTs with 86 carbon atoms (TEX_{86}) is a measure for sea surface temperature (SST), which is based on the fact that pelagic Crenarchaeota increase the relative amount of GDGTs with cyclopentane moieties in their cell membrane with increasing temperature (Schouten et al., 2002). The Branched and Isoprenoid Tetraether (BIT) index is a measure for the relative fluvial input of soil organic matter in marine sediments, based on the amount of terrestrially derived branched GDGTs in marine sediments relative to the isoprenoid GDGT crenarchaeol which is predominantly derived from marine Crenarchaeota. (Hopmans et al., 2004; Weijers et al., 2006b). Further, the relative distribution of branched GDGT membrane lipids in soils is also determined by environmental factors and reflect biological adaptations of the membranes of soil bacteria to ambient conditions. Based on a large survey of worldwide distributed soils, Weijers et al. (2007) found that the amount of cyclopentane moieties in the GDGTs, as expressed in the Cyclisation ratio of Branched Tetraethers (CBT), is a function of soil pH, and the amount of methyl groups in the alkyl chains, expressed in the Methylation index of Branched Tetraethers (MBT), depends on

both soil pH and annual mean air temperature (MAT) (Weijers et al., 2007b). Together, the MBT index and CBT ratio could therefore be used as a proxy to reconstruct annual MAT. A combined application of these GDGT based proxies could, thus, provide insight in absolute temperature development in the marine and terrestrial realm and in changes in river runoff of terrestrial organic matter and its composition.

1.3.3 Oxygen and carbon isotopes

Foraminifera build shells of calcium carbonate ($CaCO_3$). The calcium, carbon and oxygen atoms, where the shells are build from, originate from the seawater the foraminifera live in. Variability in ice volume, salinity, SST and productivity results in fractionation of the carbon and oxygen isotopes in seawater, which is recorded by the shells of the foraminifera (Ruddiman, 2001). By measuring the oxygen and carbon isotopes of benthic foraminifera, i.e. living at the sea floor (in this study *Cassidulina teretis*), may thus provide information on productivity, salinity, ice volume and SST changes.

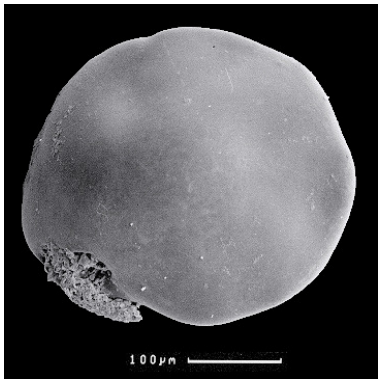

Figure 6) Photo of the benthic foraminifer *Cassidulina teretis*, used for oxygen isotope measurements (foraminifera.eu)

1.4 Hypotheses

The gamma ray and magnetic susceptibility logs, available from previous studies (Kuhlmann, 2004; Kuhlmann et al., 2006), indicate a periodical variation in lithology, characterized by alternations between finer (and darker) clay intervals and coarser silt,- to sand intervals. Based on previous palynological studies (Kuhlmann, 2004; Kuhlmann et al., 2006; Donders et al., 2009b), the clay intervals tentatively correlate with the even MIS 102, 100, 98, 96 and 94, representing cooler, “glacial” episodes. The coarse intervals tentatively correlate with the odd MIS 103, 101, 99, 97 and 95, representing warmer, “interglacial” episodes. Coinciding with the lithology we expect to find variations in the pollen and dinocyst records and the (organic) geochemical records, representing cooler and warmer episodes. Furthermore we expect to find a strong climate coupling of terrestrial and marine environments, partly based on the previous studies.

The petrochemical indices CPI and ACL, in combination with the C/N ratio and BIT index are expected to fluctuate as a result of sea level variations, i.e. differences in the amount of terrestrial vs. marine dominated organic matter input. Generally, the petrochemical CPI and ACL proxies and the C/N ratio and BIT index are believed to yield values reflecting substantial input of terrestrial organic matter.

If applicable, the novel organic geochemical proxies are expected to deliver estimates of absolute annual MAT (MBT-CBT) and SST (UK'_{37} and TEX_{86}) throughout the record, thereby determining the degree of cooling during the earliest Northern Hemisphere glaciations. Around the Pliocene-Pleistocene boundary we expect to find air temperatures comparable to those found by Donders et al. (2009a) of about 14°C for the Pliocene. Onwards a large amplitude for air temperature variations of up to ~12°C is expected, based on model outcomes of Bintanja and Van de Wal (2008) for the Early Pleistocene in North America. The modeled surface air temperatures of Bintanja and Van de Wal (2008) were up to ~11°C below present day temperatures. Therefore it is expected that reconstructed air temperatures in the glacial periods in the Early Pleistocene in northwest Europe are way below present day temperatures (e.g. MAT for the Netherlands in the period 1961-1990 was ~9.5°C; KNMI, 1997). During the interglacials of the Early Pleistocene temperatures are expected not to exceed the Pliocene temperatures of about 14°C (Donders et al., 2009a). Reconstructed SSTs are expected to show similar trends, but with a slightly smaller amplitude compared to the annual mean air temperatures because of the heat capacity of water.

2. Geological setting

During late Cenozoic times the North Sea Basin (*fig.7a*), together with the East-German Polish Basin, was part of the North West European Basin (Vinken, 1988; Ziegler,1990; Evans et al., 2003). The NW European Basin covered today's offshore and onshore parts of the Netherlands, Germany and Denmark. The basin was surrounded by landmasses, however in the north-west it had an open connection with the Atlantic Ocean (Bijlsma, 1981; Glennie, 1990; Ziegler, 1990). In the south the London–Brabant-Massif separated the North Sea Basin from the Atlantic, although at some times during the Pliocene a connection through the English Channel may have existed (Funnel, 1996).

The central North Sea Basin was filled with up to 3500 metres of siliciclastic sediments throughout the Cenozoic. About half of these sediments were deposited during the Neogene. Although the presence of hydrocarbons in the North Sea Basin generated a lot of information on North Sea geology (Parker, 1993; Fleet and Boldey, 1999; Evans et al., 2003) not much attention was paid to deposits of the Upper Neogene. Mainly due to a lack of hydrocarbon potential. The discovery of shallow gas pockets (1990s) in Neogene sediments, resulted in increased interest of the Dutch offshore sector (*fig.7b*) in the Neogene sediments, leading to a large number of high quality borehole samples. These borehole samples were used by Kuhlmann et al. (2006) to construct a solid integrated chronostratigraphy for the Upper Neogene deposits. This solid integrated chronostratigraphy is based on paleomagnetic data and dinoflagellate and foraminiferal proxies. Borehole samples taken from one of the cores (A15-3) used for the construction of the solid integrated chronostratigraphy are also used in this study.

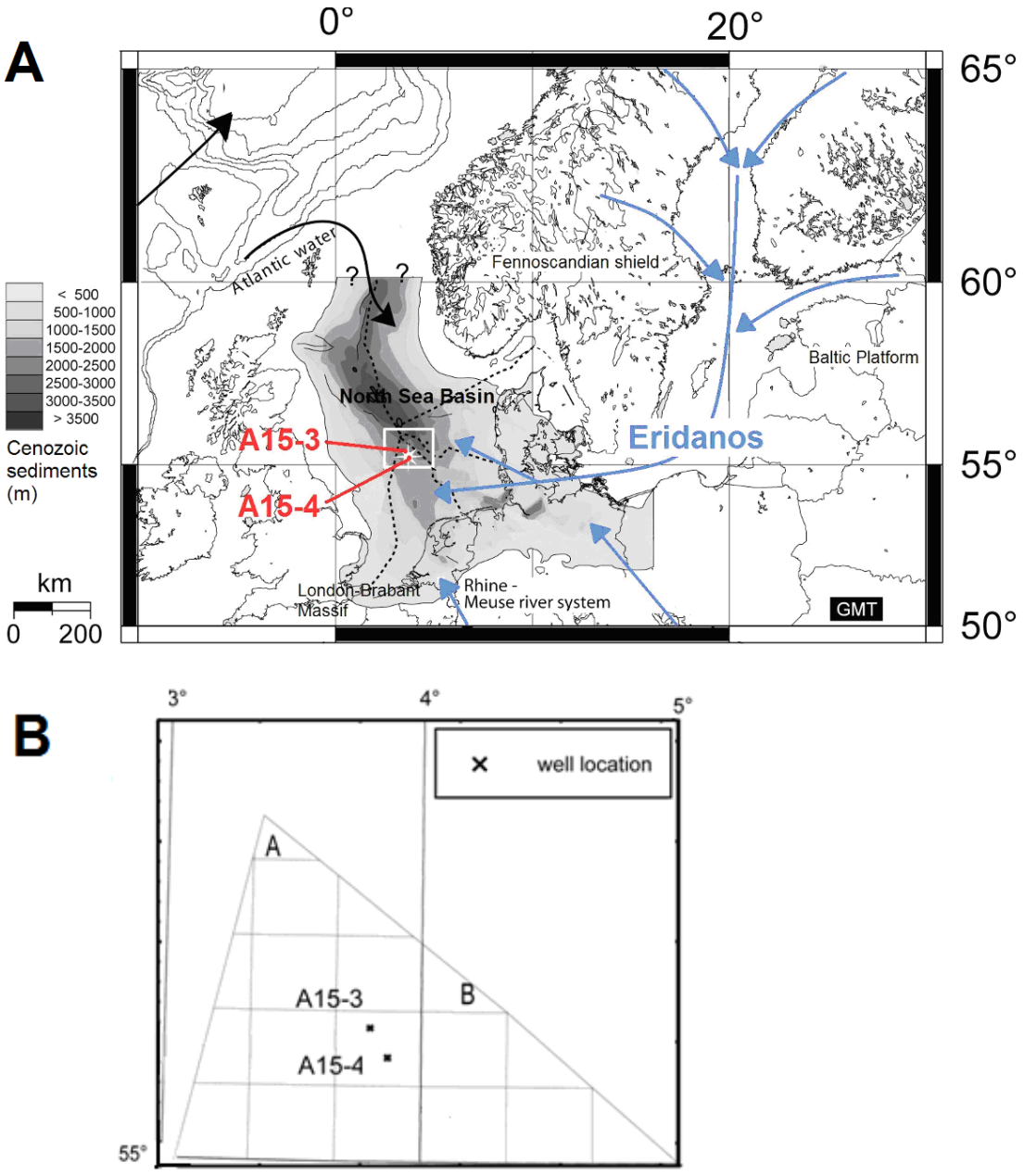

Figure 7) (a) Core locations (red) and the flow direction of the ancient Eridanos river system (blue). The dashed lines indicate the distribution of the different North Sea offshore sectors. (b) Enlargement of the NW part of the Dutch offshore sector (the AB blocks) with the exact locations of the studied cores.

Late Cenozoic sedimentation in the North Sea Basin was dominated by a large clastic depositional system, also known as the "Eridanos river system", that progressively prograded into the basin (*fig.7a*). This system probably existed since Late Oligocene times (Burger, 2002; Huuse, 2002). Originally the prograding system developed from the

north-east (the current Baltic area), after which it rotated clockwise towards a sediment transport direction from east to west over present day northern Poland, northern Germany, Denmark and The Netherlands (Sørensen et al., 1997; Michelsen et al., 1998; Clausen et al., 1999; Huuse et al., 2001). At these times, the sediments were mainly delivered by rivers draining the Fennoscandian Shield and the Baltic Platform (Bijlsma, 1981). These rivers together formed the "Baltic river system" (Zagwijn, 1989; Gibbard et al., 1991) and had an averaged drainage area of 1.100.000 km^2 (Overeem et al., 2001) The river system was active until the Late Pliocene/Early Pleistocene, when it merged with the Rhine–Meuse river system, draining from the south-east.

Progradation of the sediments resulted in several major sequences (*fig.8*) within the Cenozoic deposits in the North Sea Basin (Michelsen et al., 1998), which is discussed in Kuhlmann et al. (2006).

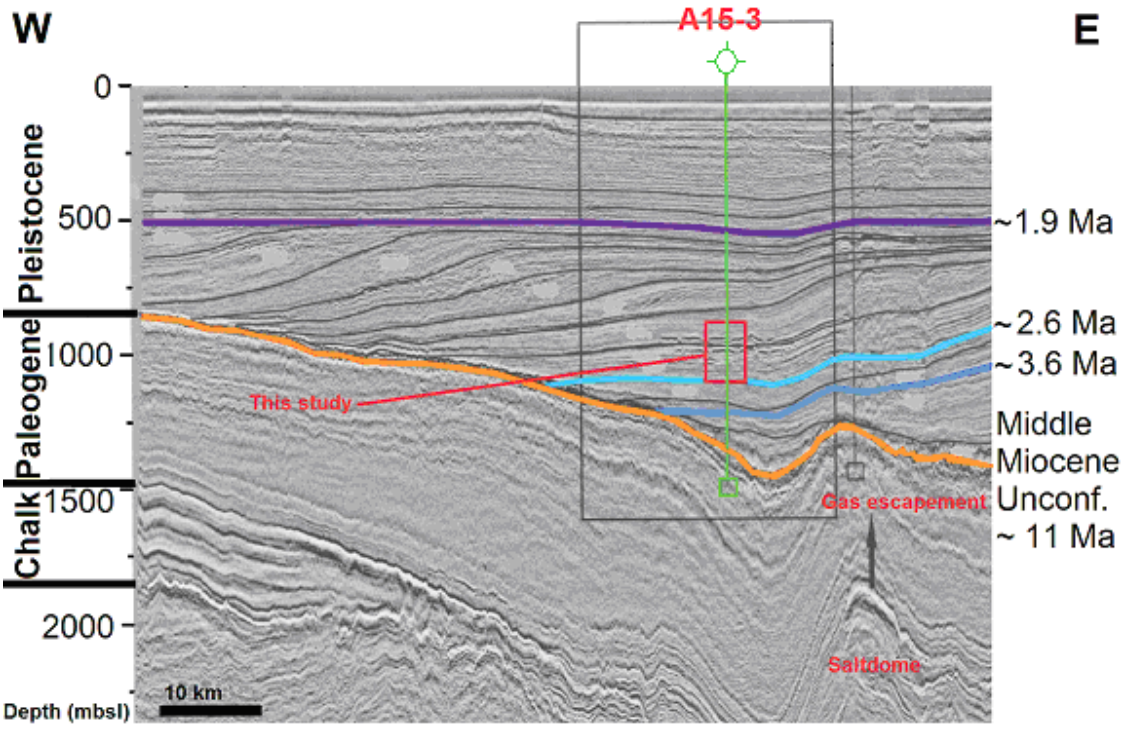

Figure 8) Seismic profile showing the progradation of the Eridanos-delta and the position of well A15-3. Modified from Kuhlman, 2004.

Since the Late Pliocene the North Sea basin rapidly shallowed and (water) depth differences were levelled off. In the Middle Pleistocene a large delta plain accumulated, covering an area of some 150.000 km^2 towards the south and east. Only in the central North Sea basin marine sedimentation continued (Cameron et al., 1993). Middle to Late

Pleistocene sedimentation was dominated by glacial-interglacial cycles. During glacials, advancing ice sheets completely altered the drainage pattern of the Eridanos river system, eventually leading the river system to cease around 450.000 years ago (Zagwijn, 1989). During glacial maxima, ice sheets reached the area more than once and glacially controlled sea level changes had profound effects on sedimentation in the shallow basin. The sedimentation became increasingly discontinuous with glacial channels occurring as common erosional features (Cameron et al., 1993; Huuse et al., 2001; Huuse, 2002).

Despite erosional features, sedimentation has been continuous at the location of cores A15-3 and A15-4 during the Early Pleistocene, which is an advantage over many terrestrial sediment archives. Another advantage of working on sediments originating from cores located on the flank of a large river delta are the relatively high sedimentation rates that provide the opportunity to obtain high resolution records, especially compared to deep sea records. A last important advantage of the used sediment cores is that both terrestrial and marine organic matter are collected at proximal sites. In combination with the already established solid integrated chronostratigraphy (Kuhlmann, 2004; *fig.9*), it makes the cores particularly suited to use for a precise terrestrial-marine correlation and a detailed reconstruction of the climate evolution and environmental development of NW Europe during the Early Pleistocene.

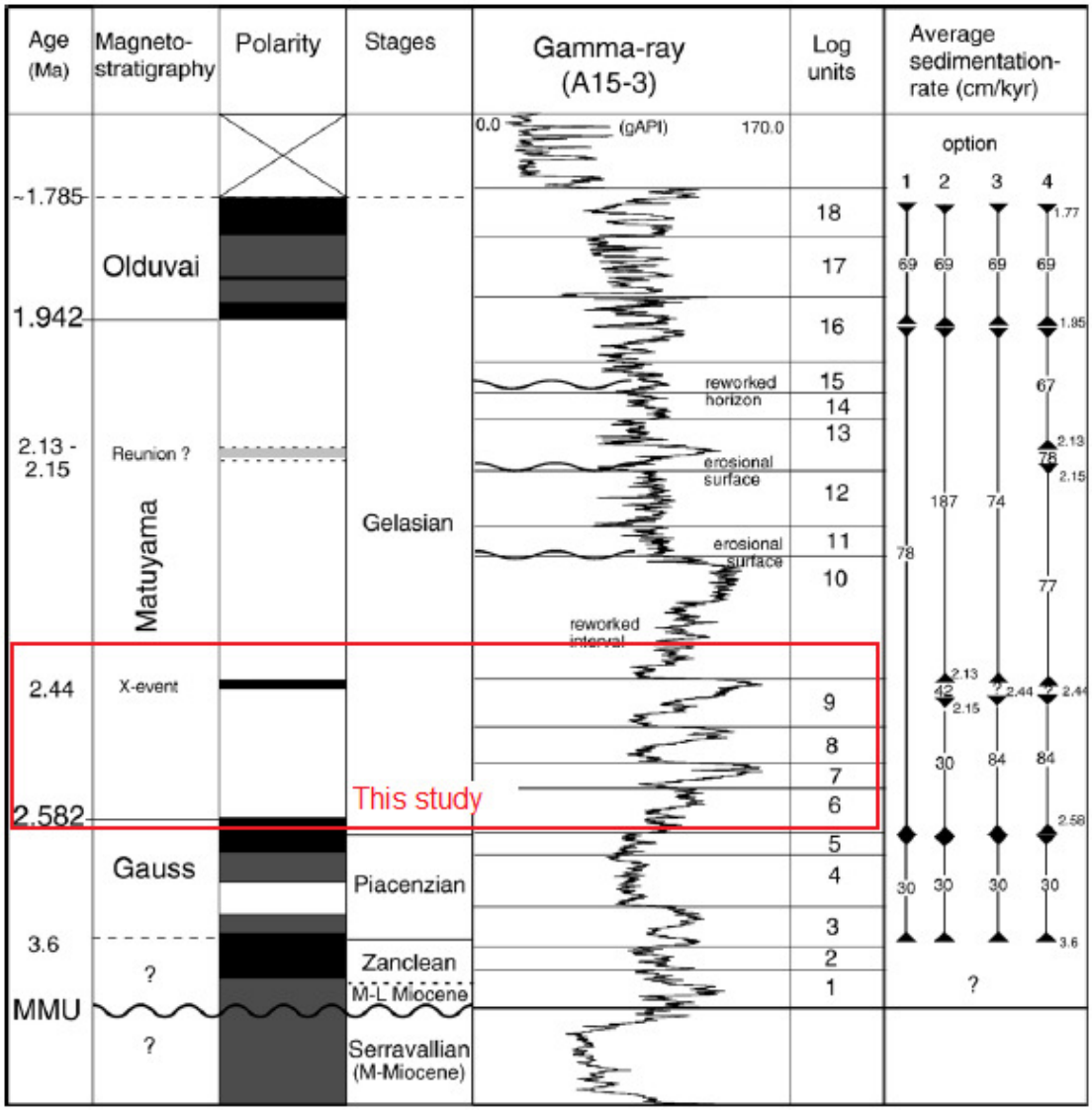

Figure 9) Integrated bio- and magnetostratigraphic chart for core A15-3, related to the logunits with respect to the standard chronostratigraphy. The right panel shows the four options for sedimentation rates. Note that the vertical scale is linear in metres, not in age (Kuhlmann et al., 2006). The red box indicates the studied interval for this high resolution multi-proxy study.

3. Materials & Methods

3.1 Samples

All sediment samples used for this study originate from the previous mentioned exploration wells A15-3 and A15-4 (*fig.7a/7b* & *Table 1*). For palynology, samples taken by Kuhlmann (2004) & Kuhlmann et al. (2006) were analyzed. For the geochemistry additional samples were taken from the cores. Most of the studied samples are core samples. A minor part of the studied samples was obtained from sidewall cores. The two boreholes were spliced on basis of the similar pattern of the gamma-ray log (*fig.2*) and equivalent biostratigraphic events, using the integrated chronostratigraphy by Kuhlmann (2004) to generate a composite record over depth. Sample depths were corrected regarding previous studies. Corrected sample depths are listed in *Appendix 2*. A15-3 was used as the reference well, the spliced depths refer to that section. After splicing, the cores were sliced in parts of one metre. Every metre of core was stored in wooden boxes (*fig.10*). Samples were taken using spoons and knifes, and collected in geochemical sample bags.

Well (core) code	A15-03	A15-04
Coordinates (x, y in UTM31, ED50 format)	552456, 6128758	557894 , 6117754
Lat/Long (°)	55.30123 , 3.8261993	55.20175 , 3.909583
End depth (m)	1400	-
Company	Wintershall B.V.	Wintershall B.V.
Begin date	28th July 1999	17th August 2001
End date	21st September 1999	28th August 2001
Objective	Exploration of hydrocarbons	Exploration of hydrocarbons
Result	Gas	Dry

Table 1) The table shows basic information of the studied exploration wells (nlog.nl).

For palynological analyses, 177 samples were studied in total (earlier work and this study*). A large part of the studied samples, 120, originate from core A15-3. The samples of A15-3 range between 400 and 1400 metres depth below sea level (mbsl). The majority of the samples, about 70, focus on the interval between 890.05 and 964.14 mbsl. This interval covers the Early Pleistocene (~2.5-2.4 Ma). The 56 studied samples from core A15-4, range between 901.72 and 1057.62 metres spliced depth, (918.4 and 1089.9 mbsl). This interval covers the Pliocene/Pleistocene transition (~2.588 Ma) and the Early Pleistocene. On the interval between 997.26 and 1037.69 metres spliced

depth, (1014.3 and 1064 mbsl) no samples were collected/studied, as a result of poor core recovery.

Almost all samples used for the organic geochemical analyses were also studied for palynology. For the organic geochemical analyses, 78 unique samples were studied. Most of these samples (41) originate from core A15-4. The studied samples range between 907.8 and 1057.62 metres spliced depth (925.45 and 1089.9 mbsl). About half of these samples (below 972 metres spliced depth) were obtained from sidewall cores. None of the 37 samples from A15-3 were obtained from sidewall cores. The studied samples range between 890.8 and 964.02 metres of depth below seafloor. Regarding the sedimentation rate of 84 cm/kilo year (ky) (*fig.9*) for the studied interval, the spacing between the samples is on average ~2 ky.

Figure 10) Part of core A15-3 stored in wooden boxes. This photo was taken on the 22th of October 2009 in a core storage of Wintershall B.V. in Beverwijk.

** In this study, pollen and spores from 55 samples (distributed over both cores) were analyzed in addition to the earlier data summarized in Donders et al. (2009b). Extensive dinocyst determinations and counts were performed during previous studies (Kuhlmann 2004; Kuhlmann et al., 2006). Dinocyst assemblages of ~15 samples were analyzed in this study to confirm trends described in previous studies. For these 15 samples only 9*

species were identified (other species were registered as indet). Of the 9 identified species, 8 are typical indicators for either warm or cold seawater temperatures.

3.2 Palynology

Preparation of the palynological samples was done according to standard marine palynological methods (e.g. Wood et al., 1996) involving HCl-HF-HCl digestion and sieving over 18 µm for both dinocysts and pollen samples. Heavy minerals were removed by flotation over zinc chloride. Dinocysts and pollen/spores were examined independently by light microscopy, using a binocular microscope, and counted up to ~100 identified cysts and ~300 pollen/spores.
Dinocyst taxonomy follows that cited in Fensome and Williams (2004). For pollen, nowadays it is widely accepted that morphological characteristics of late Pliocene to Early Pleistocene pollen types can directly be related to extant genera and families (Donders et al., 2009b). This correlation potential is a sound basis for floristic analysis of the assemblages and the recognition of similarities with modern vegetation types.

3.3 Organic geochemistry

3.3.1 Elemental analyses (TOC;C/N)

For the determination of TOC, about 0.3 g of freeze dried and powdered sediment of each sample was weighed and stored in Greiner centrifuge tubes of 15 ml. To remove carbonates, 7,5 ml 1 M HCL was added. After bubbling of gas ceases, the tubes were closed and placed on a shaker for 4 hours. After that, the acid was removed upon centrifugation. This step was repeated one more time for 12 hours on the shaker. Finally, the samples were washed twice with demineralised water and stored in an oven at 40-50℃ for 96 hours. To determine the weight loss by the removal of carbonates the dried samples were weighed again. The samples were grinded and ~15 to 20 mg per sample was weighed in tin foil cups. Measurements were performed using a Fisons NA1500 NCS elemental analyzer with a normal Dumas combustion setup. Three external standards, BCR, atropine and acetanilide, were analyzed before and after the series, and after each ten measurements. Measurements were normalized to these standards.

%TOC per gram of sediment was calculated using the following formula:

%TOC = C% * W2/W1

C% = result of NCS analyzer
W1 = weight of sample before decalcification
W2 = weight of sample after decalcification

3.3.2 Sample processing (for biomarkers)

In organic geochemistry it is of great importance to work 'clean'. This means that solvents used during the extraction and measurement of samples and cleaning of laboratorial equipment need to be checked for contamination (e.g. plasticizers). Every new bottle of solvents is checked for contamination by evaporating down 50ml redissolving this in 50µl, and injection on a gas chromatograph. When no contamination is found the solvents can be used. The most commonly used solvents in the laboratory include dichloromethane (DCM; CH_2Cl_2), methanol (MeOH, CH_3OH), *n*-hexane (C_6H_{14}), propanol (C_3H_8O) and ethyl acetate ($C_4H_8O_2$).
Another important lab procedure is the cleaning of glassware and other equipment (e.g. tweezers) that may come in contact with samples. First everything is washed under hot water with detergent. Afterwards it is soaked (at least overnight) in demineralised water containing 2-5% Extran. Subsequently it is rinsed three times with tap water and three times with demineralised water. equipment is dried using an oven (120°C for 1-2 hours) or on a drying rack. Finally, openings of glassware are sealed off with aluminium foil. Before using the glassware, it is rinsed two times with MeOH and two times with DCM. Generally, all lab work was performed according to regulations stated in the Laboratory manual Marine Organic Biogeochemistry NIOZ, Version 11, 2008.

For the analysis of biomarkers, of each sample about 10 g of sediment was freeze dried and mechanically powdered. The sediments were extracted with a DCM : MeOH solvent mixture (9:1, v/v, 3 times for 5 minutes each) using an Accelerated Solvent Extractor (ASE, Dionex 200)* at 100°C and ca. 7.6 x 10^6 Pa. The resulting Total Lipid Extract (TLE) was evaporated to near dryness using a rotary evaporator under near vacuum. The TLE then was transferred to a 4 ml vial and dried under a continuous N_2 flow.

Afterwards, 1 ml of DCM was added after which 0,5 ml (~50% of the TLE) was saved as archive. The other 'working part' was desulphurized. For the desulphurization cupper turnings were activated by adding a small amount of 2M HCl. The acid was pipetted off, and the cupper turnings were washed with demineralised water until the pH of the water was neutral. Afterwards the cupper turnings were washed twice with a small amount of methanol and DCM successively. Together with some DCM, the cupper turnings were added to the TLE, and after addition of a small stirring bar, the TLE was stirred overnight. The next day, the DCM layer was filtered over a small pipette filled with Na_2SO_4 to remove the CuS. The resulting desulphurized TLE was separated over a small column (Pasteur pipette) packed with activated Al_2O_3. Activation of the Al_2O_3 was performed by heating the Al_2O_3 in an oven for 2 hours at 150°C. Before the separation, the column was conditioned by flushing with one column volume of *n*-hexane : DCM 9:1 (v/v). The TLE was separated into an apolar fraction (*n*-alkanes), a ketone fraction (alkenones) and a polar fraction (GDGTs) by eluting with three column-volumes of *n*-hexane : DCM 9:1 (v/v), *n*-hexane : DCM 1:1 (v/v) and DCM : MeOH 1:1 (v/v) solvent mixtures, respectively. A flowchart which summarizes these steps is shown in *figure 11*.

** Two samples were also ultrasonically extracted using successively less polar solvents (methanol, methanol: DCM 1:1 (v/v), and DCM), 3 times for 5 min each.*

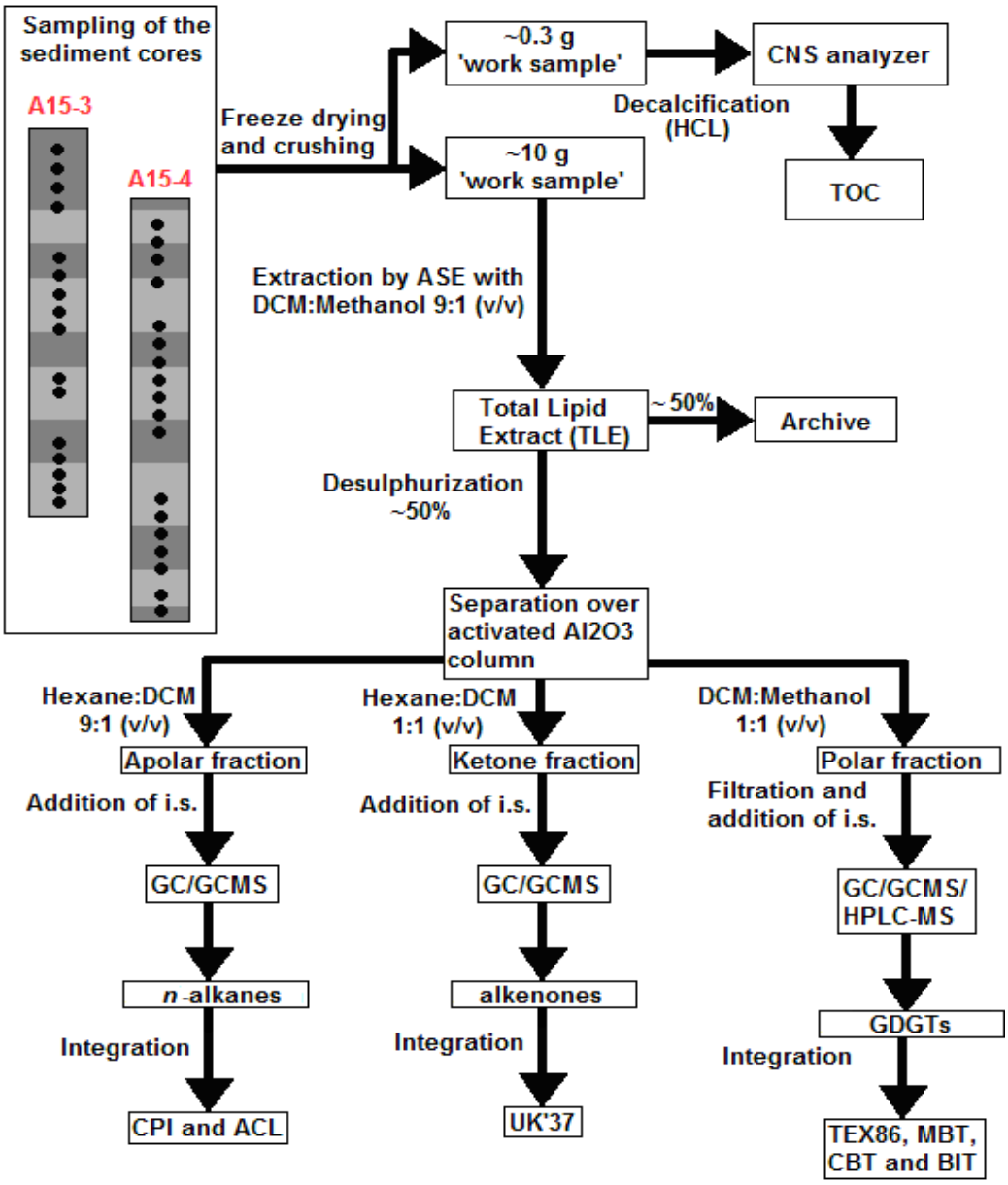

Figure 11) Flowchart for the organic geochemical analyses.

3.3.3 n-Alkane and Alkenone analyses (GC and GCMS)

Both fractions, containing *n*-alkanes and alkenones respectively, were analyzed by gas chromatography (GC) and gas chromatography/mass spectroscopy (GC/MS). GC was used for quantification of the compounds, which was achieved by integrating the peak areas of the different compounds in the chromatogram and comparison with the peak areas of the internal standards. The components of both fractions were identified based on retention times and mass spectrum, using GC/MS.

For the GC, samples were dissolved in 55 µl hexane and analyzed using a Hewlett Packard G1513A autosampler interfaced to a Hewlett Packard 6890 series Gas Chromatography system using a CP-Sil-5 fused silica capillary column (25 m x 0.32 mm, film thickness 0.12 µm), with a 0.53 mm pre-column. Temperature program: 70°C to 130°C (0 min) at 20°C min^{-1}, then to 320°C at 4°C min^{-1} (hold time 20 mins), which results in a total time of 71 minutes per analysis. Injection volume of the samples was 1 µl. GC/MS analyses were performed on a ThermoFinnigan Trace GC ultra interfaced to a ThermoFinnigan Trace DSQ MS using the same temperature program, column and injection volume as the GC.
Quantification was achieved using standards added prior to analysis. Two internal standards were added to the apolar fraction. Heptatriacontane (C_{37}) was added to indentify and quantify the *n*-alkanes present in the apolar fraction. 5α-androstane was solely used for quantification. For both standards about 2000 ng was added. This amount was chosen to obtain a good signal. One standard, 2-nonadecanone, was added to the ketone fraction for quantification. To obtain a useful signal, again, about 2000 ng of standard was added.

The Carbon Preference Index (CPI) was calculated for the *n*-alkanes C_{25}-C_{33} with the following formula:

$$\mathbf{CPI = [0,5\ \Sigma\ ([C_{25}]+[C_{27}]+[C_{29}]+[C_{31}]+[C_{33}])\ /\ \Sigma\ ([C_{24}]+[C_{26}]+[C_{28}]+[C_{30}]+[C_{32}])\ +\ 0,5\ \Sigma\ ([C_{25}]+[C_{27}]+[C_{29}]+[C_{31}]+[C_{33}])\ /\ \Sigma\ ([C_{26}]+[C_{28}]+[C_{30}]+[C_{32}])+[C_{34}])]}$$

The average chain length (ACL) was calculated for the n-alkanes C_{27}-C_{33} with the following formula:

$$\mathbf{ACL_{27\text{-}33} = (27[C_{27}]+29[C_{29}]+31[C_{31}]+33[C_{33}])\ /\ ([C_{27}]+[C_{29}]+[C_{31}]+[C_{33}])}$$

The relative abundance of the C_{23} *n*-alkane (biomarker for Sphagnum) was calculated using the following formula:

$$\mathbf{Relative\ abundance\ of\ C_{23} = [C_{23}]/\ (([C_{27}]+[C_{29}]+[C_{31}]\ ]+[C_{33}])/4)}$$

The unsaturated ketone index, UK'_{37}, was calculated using the following formula:

$UK'_{37} = [C_{37:2}] / [C_{37:2} + C_{37:3}]$ (Prahl and Wakeham, 1987)

Note: The numbers refer to the compounds which are illustrated in figure 4.

The obtained UK'_{37}-value was used to calculate SST, applying the following calibration:

$SST = (UK'_{37} - 0{,}044) / 0{,}033$ **(**R^2=0.958) (Müller et al., 1998)

3.3.4 GDGT analyses (HPLC-MS)

To the polar fraction, containing the GDGTs, 500 ng of the C46 GDGT internal standard was added. The polar fraction was ultrasonically dissolved in *n*-hexane : propanol (99/1, v/v) and filtered over a 0.45 µm mesh PTFE filter (ø 4mm) prior to analysis. GDGTs were analyzed using high performance liquid chromatography / atmospheric pressure chemical ionization–mass spectrometry (HPLC/APCI-MS), according to methods of Hopmans et al. (2000, 2004), with minor modifications. Analyses were performed on an Agilent 1100 series/Hewlett-Packard 1100 MSD SL series instrument, equipped with auto-injection system and HP-Chemstation software. Separation was achieved on a Prevail Cyano column (150 mm x 2.1 mm, 3 µm; Alltech). The flow rate of the hexane:propanol (90:10, v/v) eluent was 0.2 ml min-1, isocratically for the first 5 min, thereafter with a linear gradient to 18% propanol in 45 min. Injection volume of the samples was 10 µl. To increase sensitivity, selective ion monitoring (SIM) of the protonated molecular ions of the GDGTs was used (cf. Schouten et al., 2007). Relative quantification of the GDGT compounds was achieved by integrating the peak areas in the mass chromatograms and comparison to the internal standard.

The BIT index was calculated using the formula:

BIT = ([1022]+[1036]+[1050]) / (([1022]+[1036]+[1050]+[Cren])
(Hopmans et al., 2004)

Note: Numbers refer to m/z values of the compounds which are illustrated in figure 5. Cren = Crenarcheol.

The Tetraether index of GDGTs with 86 carbon atoms, TEX_{86}, was calculated using the following formula:

TEX_{86} = ([1298]+[1296]+[1292']) / (([1300]+[1298]+[1296]+[1292'])
(Schouten et al., 2002)

The obtained TEX_{86}-value could subsequently be translated into a SST estimate using the following calibration formula provided by Kim et al. (2008):

SST= -10,78 + 56,2 × TEX_{86} (R^2 = 0.935)

The MBT index and CBT ratio are defined as follows (Weijers et al., 2007b):

MBT = ([1022]+[1020]+[1018]) / (([1022]+[1020]+[1018]) + ([1036]+[1034]+[1032]) + ([1050]+[1048]+[1046]))

CBT = - LOG(([1034]+[1020])/([1036+1022]))

These can be translated in a soil pH estimate and an estimate for annual mean air temperature using the following calibration formulas (Weijers et al., 2007b)::

pH = (3,33-CBT)/0,38 (R^2 = 0.70)

MAT = (MBT - (0,122 + 0,187 × CBT)) / 0,02 (R^2 = 0.77)

3.4 Oxygen and carbon isotopes

Oxygen and carbon isotopes were measured on the carbonate remains of *Cassidulina teretis*, a species of benthic foraminifera that is generally occurring throughout the cores. Between ~20 and 50 µg of specimen per sample was weighed after which the isotopes of the carbonate were measured using a Kiel III device coupled to a 253 ThermoFinnigan MAT instrument. Isotope measurements were normalized to an external standard 'NBS-19'.

4. Results

4.1 Palynology

The pollen records (*fig.12*) for both cores show assemblages dominated by *Pinus* pollen. Since *Pinus* pollen are typically wind-transported, it is very difficult to use them for a paleoenvironmental interpretation. Although some trends can be observed, no clear picture can be drawn based on the *Pinus* pollen. The second important element of the pollen assemblages is Ericaceae, showing higher abundances in the clay intervals. These increases are also (partly) visible for *Sphagnum*, Poaceae and the freshwater algae *Pediastrum*. The increases of these water-transported pollen indicate a more open landscape, as Ericaceae and Poaceae are typical indicators for heath,- and grassland vegetation. This open landscape can be associated with a colder and drier climate related to the first large icecap formations in the Northern Hemisphere. On the contrary, *Picea*, *Tsuga*, *Sciadopitys*, *Dryopteris* and *Osmunda* show higher abundances (relative to the pollen sum) in the coarser-grained intervals, indicating warmer and wetter conditions during deposition of these intervals, which would be expected during interglacial stages. Furthermore, the limited occurrence of *Taxodium,* only present in the lowermost stages, MIS 103 and MIS 102, is important.

Taxodium is typical swamp vegetation occurring in warm-temperate and subtropical climates. Presently, *Taxodium* is extinct in Europe and occurs only in the southeast of the US, where it is native to humid climates with precipitation ranges between 760 mm/y and 1630 mm/y. Although it grows best in warm climates, the current natural northern limit of the species is not determined by annual mean temperature, but related to specific reproductive requirements. The most important parameter in this is the occurrence of winter frost, because this prevents regeneration of seedlings by ice damage. Larger trees, nevertheless, are able to tolerate much lower temperatures and lower humidity (Farjon, 2005). The disappearance *of Taxodium* in MIS 102 therefore indicates a (severe) cooling of the climate, at least for winter conditions. It is important to note that palynology does not correlate with lithology very strictly. In the coarser intervals, representing MIS 99 and 95, we observe rather high abundances of Ericaceae, although these are mainly attributed to cooler, glacial conditions. Vice versa similar situations appear, e.g. relatively high abundances of *Picea*, *Sciadopitys* and *Osmunda* during the clay interval representing the “glacial” MIS 94. However in the greater context,

palynology supports the hypothesis that the coarser intervals represent warmer periods (interglacials) and the clay intervals colder periods (glacials).

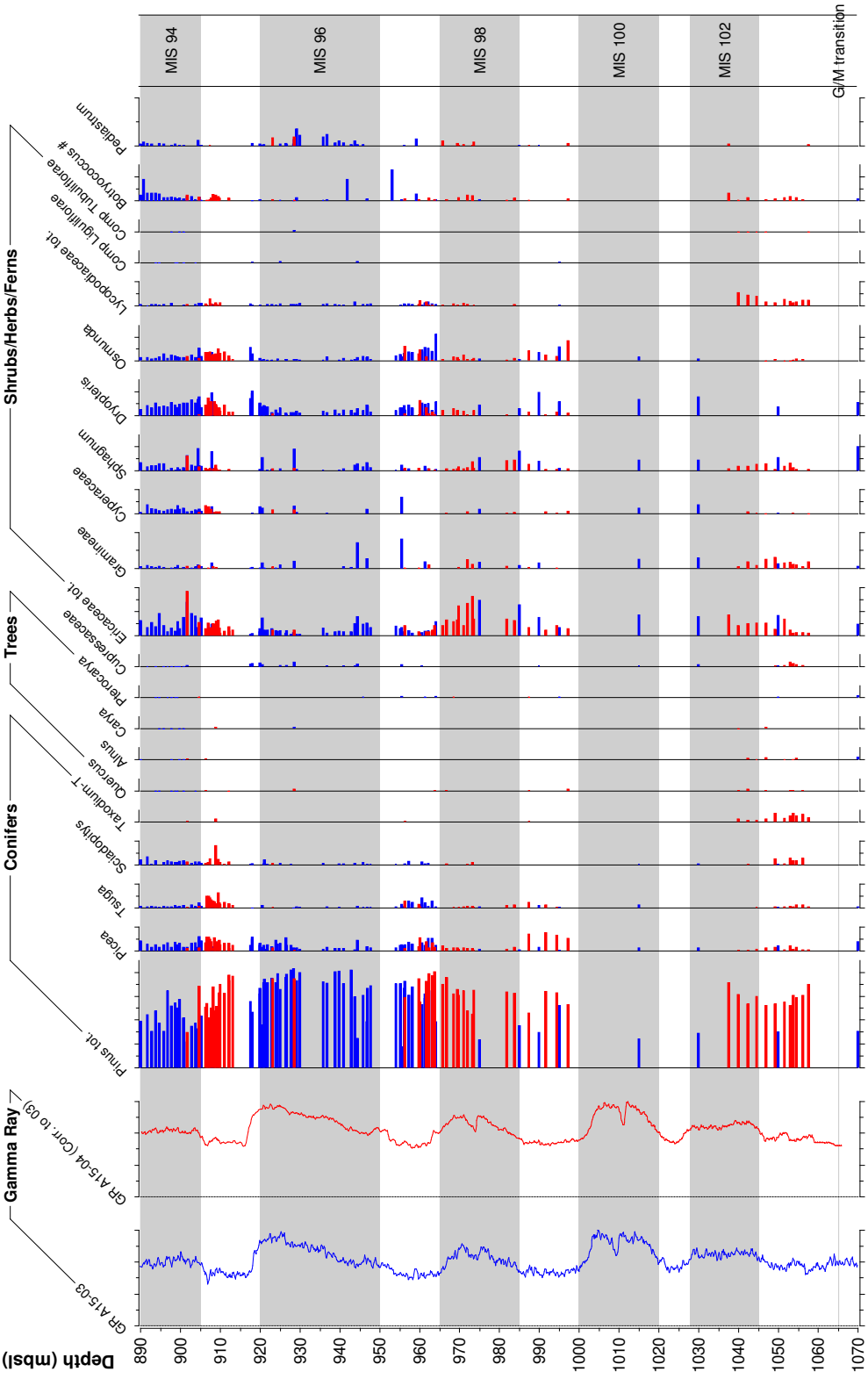

Figure 12) Gamma ray and pollen diagram of A15-03 (blue bars) and A15-04 (red bars, on spliced depth scale). Gauss/Matuyama (G/M) transition is based on the paleomagnetic data of A15-03 in Kuhlmann(2004). Grey bars indicate the correlation of the GR and dinocyst signals to the MIS as proposed in Kuhlmann (2004), the exact phase relation is discussed further in section 4

The distribution of the scanned dinocyst assemblages (*fig.13*) confirms trends described in previous studies (Kuhlmann, 2004; Kuhlmann et al., 2006). Although only the upper part of the studied section was scanned, dinocyst assemblages clearly show the dominance of “warm taxa” (mainly *Operculodinium israelianum*) in the coarser grained intervals. Only one clay interval was covered entirely, this interval was however dominated by “cool taxa”. It is important to note that many cysts were fragmented and that palynology does not follow lithology one to one, e.g. *Operculodinium israelianum* domination in the lower part of the upper clay interval.

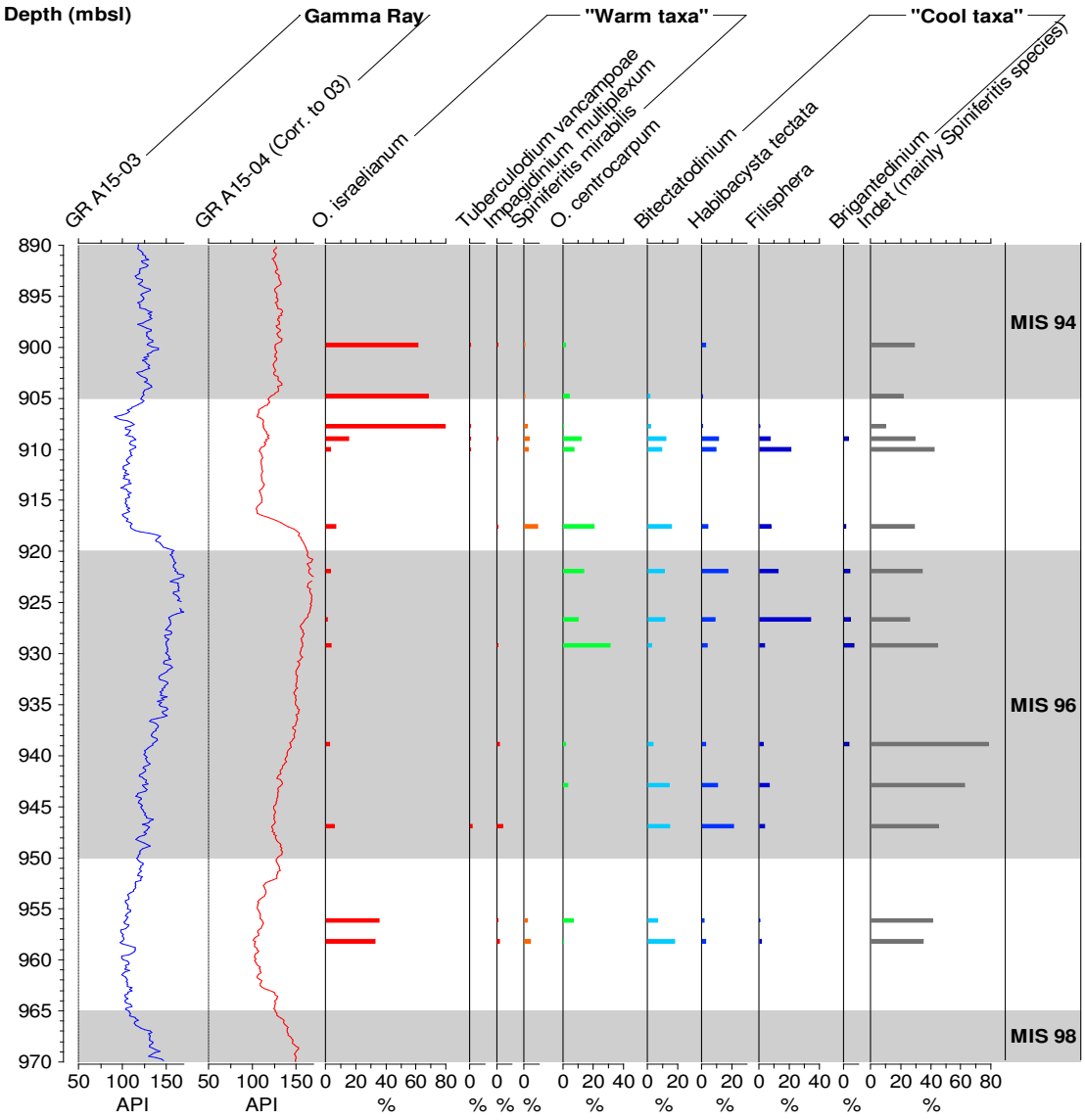

Figure 13) Gamma ray and (scanned) dinocyst distributions for the upper part (890-970 mbsl) of the studied section.

4.2 Organic geochemistry

4.2.1 Elemental analyses (TOC;C/N)

The TOC data show a very strong trend related to lithology (*fig.14*). The observed TOC trend is quite remarkable as it seems opposite of what normally would be expected in these kind of sediments, i.e. higher TOC values would be expected for the darker clay intervals and lower values for the coarser sand,- siltstone intervals. Here, however, lowest TOC contents are reached in the clay intervals with values of ~0.5%, ~0.5%, ~0.25% and ~0,4% for MIS 102, 98, 96 and 94, respectively. The maxima are reached in the coarse intervals with values of ~1.1%, ~1%, ~1% and ~0.9% for MIS 103, 99, 97 and 95, respectively . Seen over the whole record, there is a minor trend suggesting a slight decrease in TOC going upwards in the section.

In contrast with TOC, total nitrogen remains rather constant throughout the section, with minima around 0.07% and maxima around 0.13%. The rather constant total nitrogen values results in a trend for the atomic C/N ratio comparable to that of TOC. In the coarser intervals the C/N ratio ranges between ~14 and 17 and in the clay intervals C/N ratios are around ~8-9. The C/N ratio for MIS 96 is an exception with values reaching as low as about ~3.5.

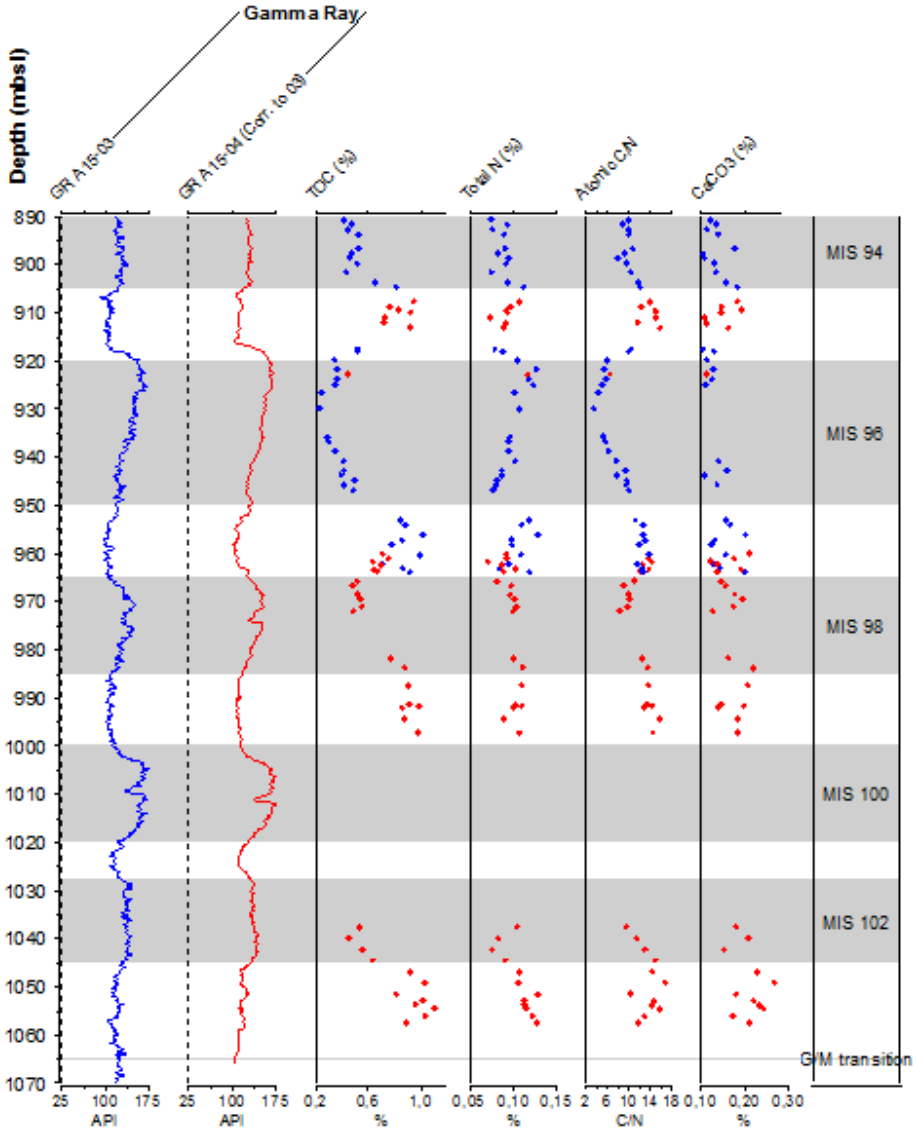

Figure 14) Diagram showing TOC, total nitrogen, atomic C/N and $CaCO_3$ data. Blue represent samples from core A15-3 and red from A15-4.

4.2.2 Apolar fractions

The chromatogram shown in *figure 15* is typical for the apolar fractions of both cores. The chromatogram is clearly dominated by plant wax-derived long chain *n*-alkanes (C_{25}–C_{35}) showing a strong odd-over-even predominance. Other compounds that are present in these fractions are hopanes and steranes, cell membrane rigidifiers for bacteria and plants, respectively, but these are very low in abundance and often difficult to identify and quantify.

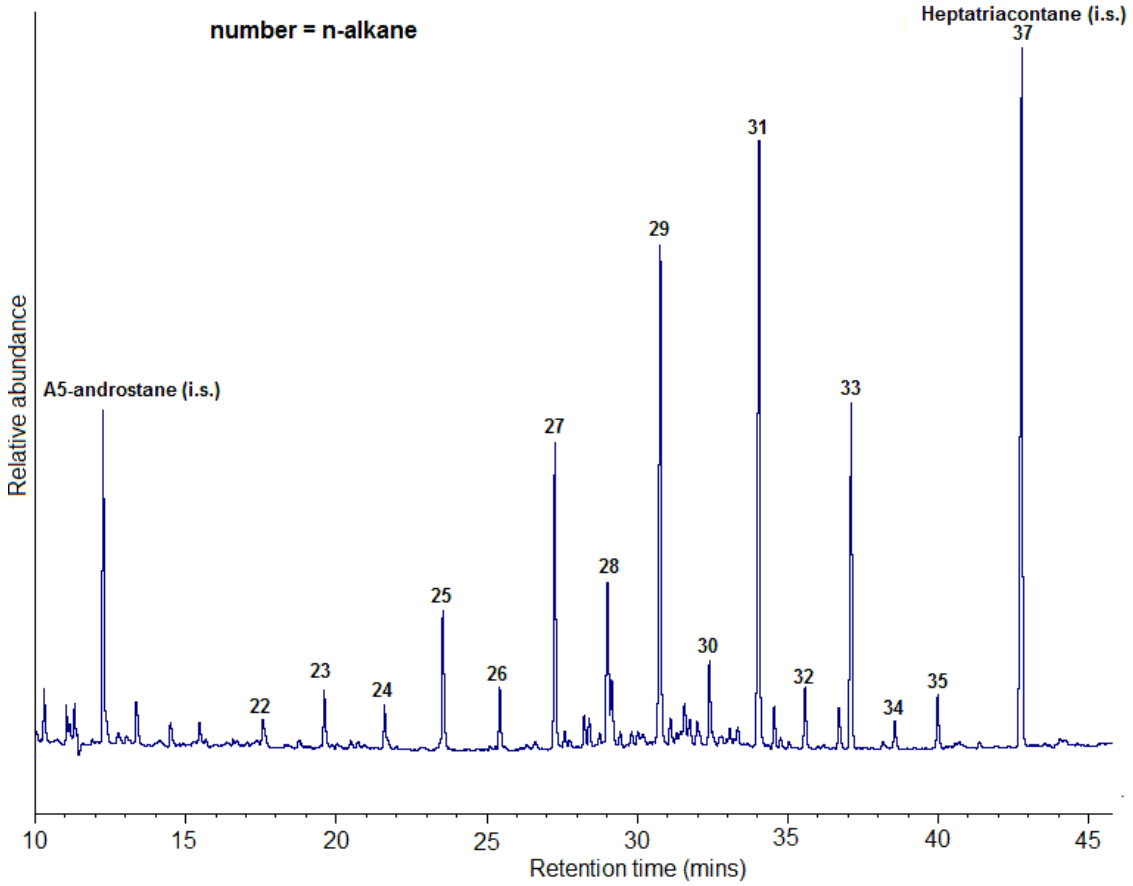

Figure 15) Partial gas chromatogram of an apolar fraction, typical for this study, of the total lipid extract from a A15-4 sample (911.06m spliced depth, 928.75 mbsl).

The CPI varies throughout the record (*fig.16*). Minimum values are around ~2.8-2.9 and are mainly situated at the transitions between the coarser sediments and the clay intervals. Maxima, around ~4.5, appear in the clay intervals, mainly in the latter part around the transition zones to the coarser intervals.

For ACL we see a similar picture, but trends are exactly mirrored. So minima in ACL (~29.3) correlate with maxima in CPI, and vice versa (maxima in ACL are around ~29.8).

The relative abundance of C_{23} *n*-alkane is highest in the clay intervals and lowest in the coarser grained intervals.

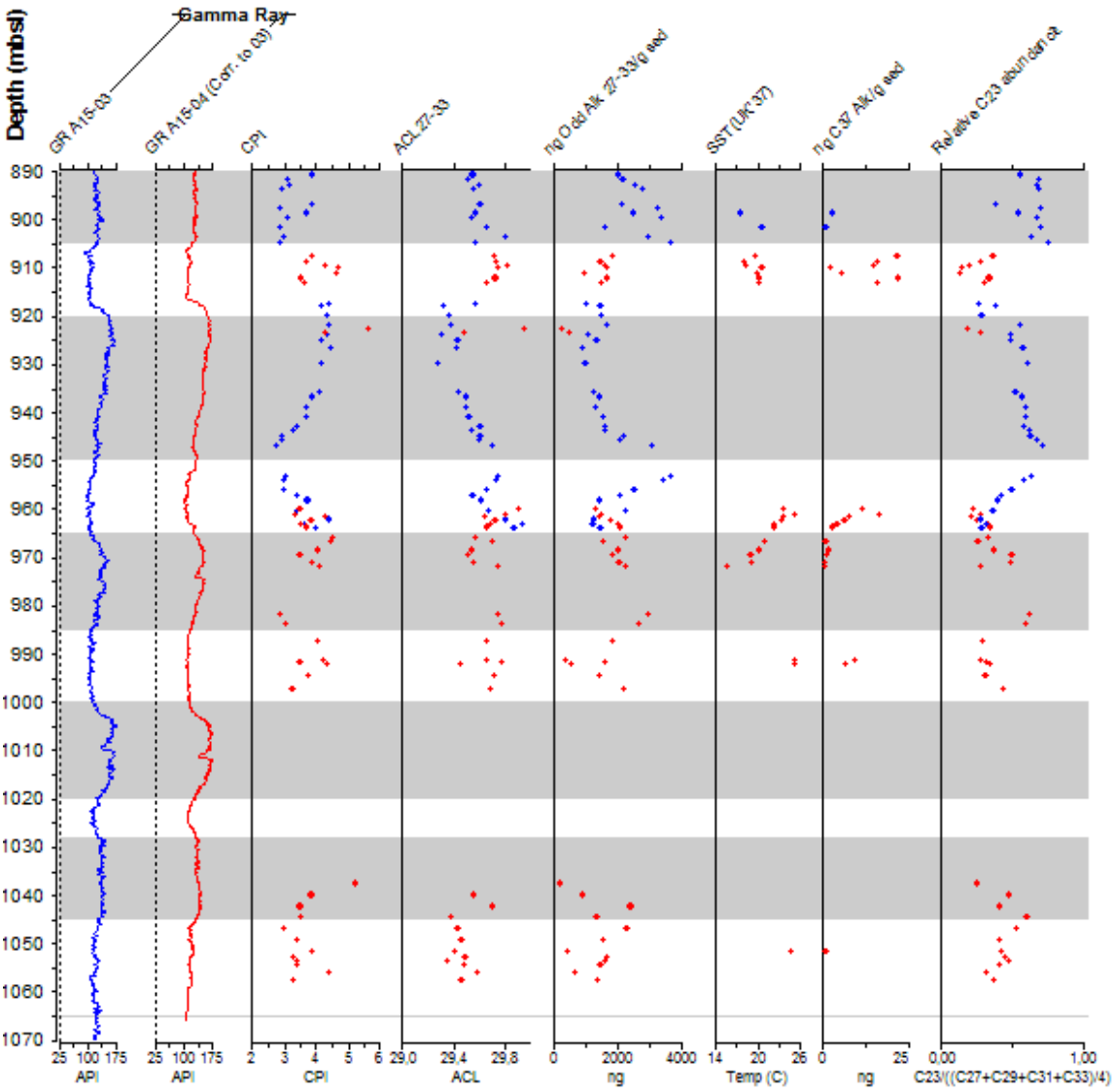

Figure 16) Diagram showing n-alkane data (CPI and ACL values as well as concentrations), alkenone data (concentrations and SST estimates based on UK'$_{37}$) and relative C_{23} abundances. Blue represent samples from core A15-3 and red from A15-4. The green arrow indicates values indicative for more marine conditions.

4.2.3 Ketone fractions

Long chain alkenones (*fig.17*) could be detected and quantified in only 23 samples (on a total of 78); 21 in core A15-4 and 2 in core A15-3 (*fig. 16*). For the A15-4 samples two clusters can be recognized. From 907.8 to 913.21 metres spliced depth, and from 960.1to 972 metres spliced depth. The reconstructed SSTs, using the UK'$_{37}$ proxy, range between ~16℃ and ~25℃.

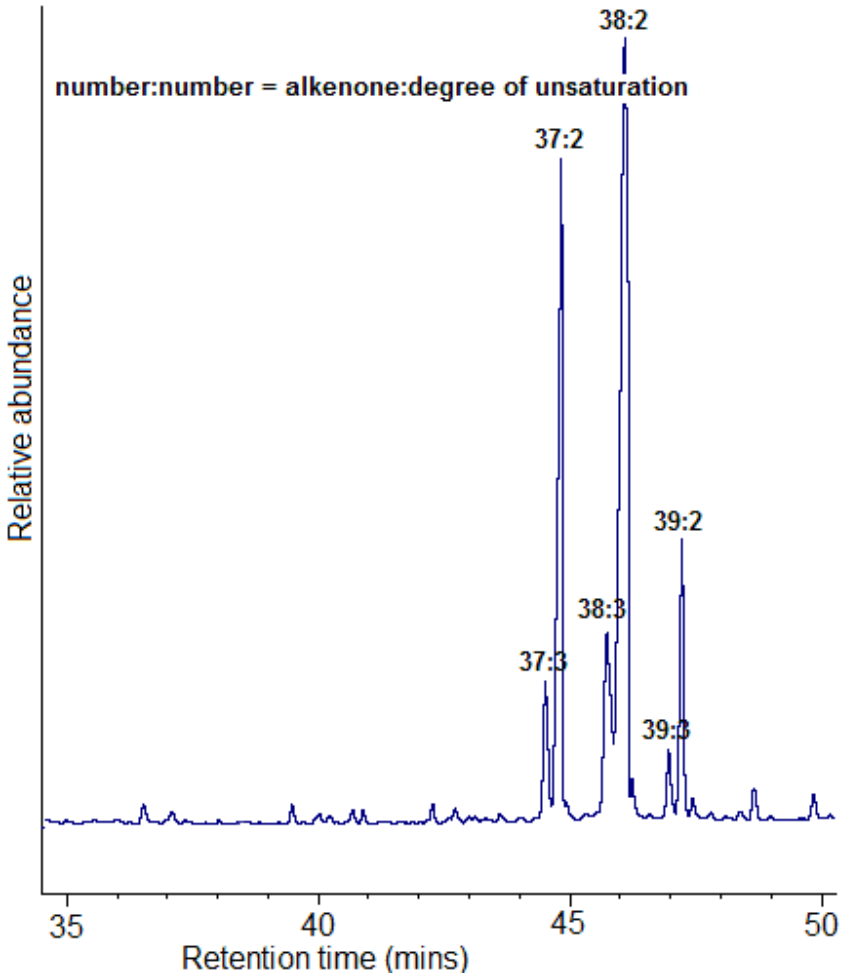

Figure 17) Partial gas chromatogram of a ketone fraction, containing the alkenones, of the total lipid extract from a A15-4 sample (960.1m spliced depth, 975.1 mbsl).

4.2.4 Polar fractions

The polar fractions were measured using HPLC/MS in two distinct runs to quantify both isoprenoid and branched GDGTs. An overview of different base peak chromatograms representing a low and a high MAT estimate and a low and a high SST estimate is shown in *figure 18*.

Note: The data obtained from the two ultrasonically extracted samples are not incorporated in the 'working dataset'. The ultrasonically extracted samples show much offset compared to the ASE-samples. To obtain a more or less constant method only the ASE-samples are used.

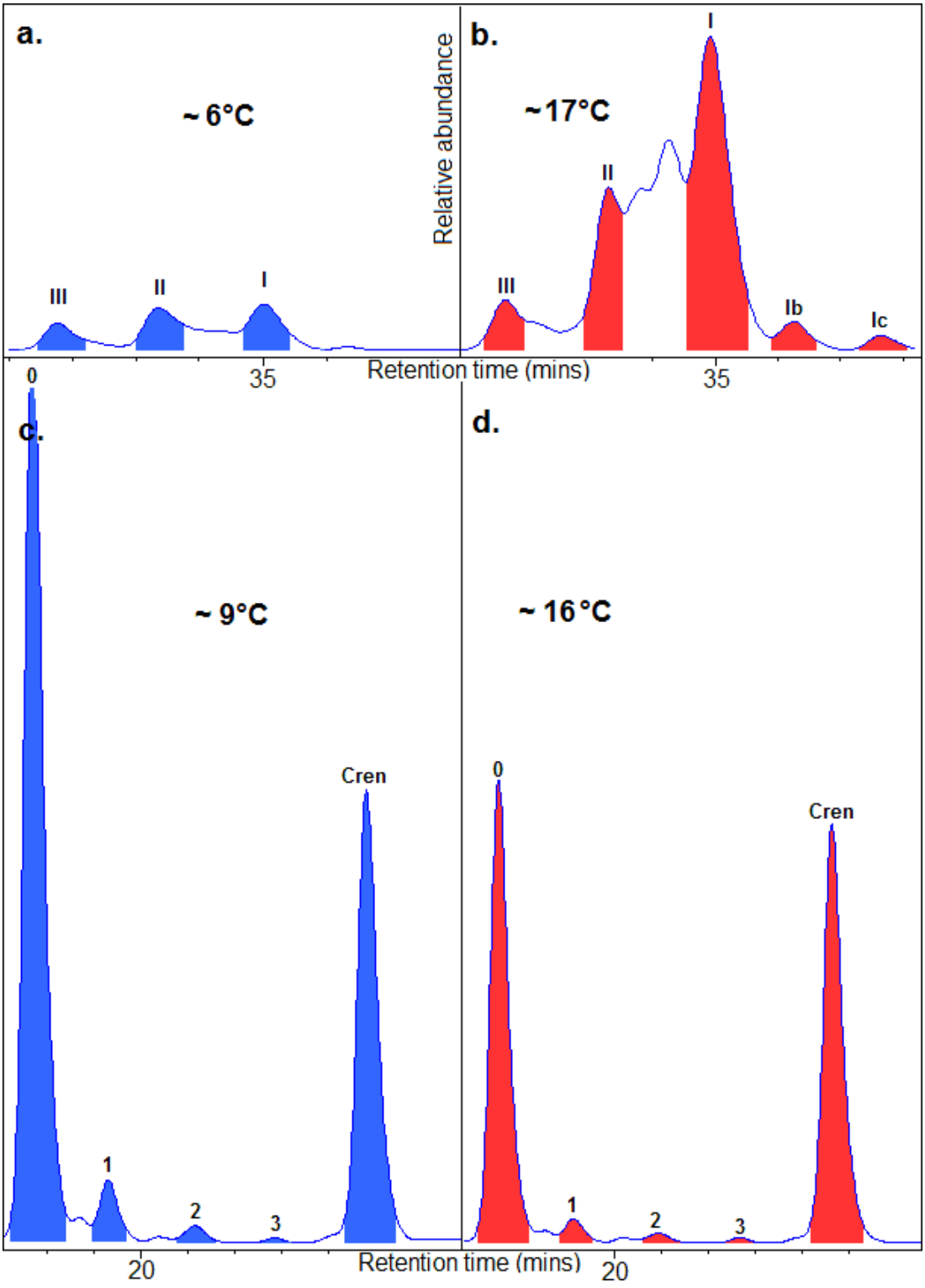

Figure 18) Overview of different HPLC/MS base peak chromatograms, showing the relative abundances of the branched GDGTs in a sample reflecting (a.) a lower MAT estimate (A15-4 997.26m spliced depth, 1014.3 mbsl, reconstructed MAT of 6,41℃) (b.) a higher MAT estimate (A15-4 968.5m spliced depth, 983.5 mbsl, reconstructed MAT of 17,40℃) and base

peak chromatograms, showing the relative abundances of the isoprenoid GDGTs in a sample reflecting (c.) a lower SST estimate (A15-4 991.72m spliced depth, 1008.35 mbsl, reconstructed SST of 8,81°C) (d.) a higher SST estimate (A15-3 942.9 mbsl, reconstructed SST of 16,21°C). Numbers and Roman numerals refer to the structures drawn in *Figure 5*.

From *figure 18* it becomes clear that the peaks representing the individual branched GDGT abundances are quite complicated. At present the cause of these awkward peaks is studied (Hopmans et al. unpublished results). Possible causes might be isomers, degradation of components or pollution. Fortunately the far majority of the HPLC/MS chromatograms used in this study is similar. In combination with consistent integration, reconstructed temperature trends will not be influenced. However the uncertainty for reconstructed absolute temperatures will increase a little.

For 16 (on a total of 78) samples no or hardly any GDGTs were detected and quantified. For the other samples all GDGTs were detected. GDGT abundances are in general low for the clay intervals and higher for the coarser intervals. Concentrations of GDGT-0 range between ~22 ng/g dry weight sediment (dws). and ~925 ng/g dws, isoprenoid GDGT concentrations range between 2 ng/g dws to 110 ng/g dws, crenarchaeol ranges between ~1 ng/g dws to ~1090 ng/g dws and branched GDGT concentrations range between ~2 ng/g dws to ~600 ng/g dws. The BIT index ranges between 0.02 and 0.73. The BIT index seems to be fairly constant (~0.5) for the lower part of the section around the Pliocene-Pleistocene transition. From MIS 99 onwards BIT is fluctuating. Minima occur mainly in the coarser intervals. On the contrary, maxima are harder to qualify. Some trend is visible in the upper part of the section. This trend is most clear in MIS 96 and the transition to MIS 95. During MIS 96 a gradual increase in BIT can be observed, from ~0.2 to ~0.65 followed by a sharp decline to 0.02 on the transition from MIS 96 to MIS 95. A similar trend can be recognized for MIS 98/97.

The relative abundances of the individual isoprenoid GDGTs differed from sample to sample as illustrated in *figure 19*. These differences are quantified (*fig.20*) with the TEX_{86} index, which varies between 0.35 and 0.51. The obtained TEX_{86} values were translated to SSTs ranging between ~9°C and ~17°C. As small amounts of isoprenoid GDGTs also occur in soils, a high input of soil organic matter (represented by a high BIT index) could comprise the use of the TEX_{86} proxy for SST reconstruction (Weijers et al., 2006b). Therefore, SST estimates based on TEX_{86} have been determined for only 21 out of 78 samples as the BIT index for these samples was <0.4 and the influence of soil derived isoprenoid GDGTs is likely to be minimal. SST values reach minima, approximately 9°C, in the coarser intervals. Around the transitions from coarse to clay intervals SST values

seem to show a large increase to temperatures around ~16-17°C. Since UK'_{37} and TEX_{86} are both SST proxies, they were supposed to yield similar outcomes. Although for both proxies few samples were suited for SST reconstructions it is clear that UK'_{37} and TEX_{86} are totally different, concerning both amplitude and temperature trends.

The relative abundances of the individual branched GDGTS also differed from sample to sample as illustrated in *figure 19*. These differences are quantified (*fig.20*) with the MBT index which varies between 0.41 and 0.73, and the CBT ratio, showing values between 0.56 and 1.03. The CBT values translate to pH values between 6.1 and 7.3 and CBT and MBT values together translate to MATs between ~6°C and ~21°C. Reconstructed annual MAT shows some remarkable trends. In the lower part of the section, temperatures are quite constant and fluctuate around 15°C, these values are comparable with temperatures reconstructed for the Late Miocene and Early Pliocene in the same area (Donders et al., 2009a). From MIS 99 onwards, temperature fluctuations are much larger and a general trend unfolds. Minima are reached in the coarse intervals, with temperatures of 6.5°C, 9.5°C and 8°C for MIS 99, 97 and 95 respectively, followed by rapid increases to reach maxima around the transitions from the coarse intervals to the clay intervals. The maximum temperatures reached are 16.5°C, 21°C and 17°C for MIS 99, 97 and 95, respectively. After a maximum, temperature decreases slowly across the clay interval to the next minimum again.

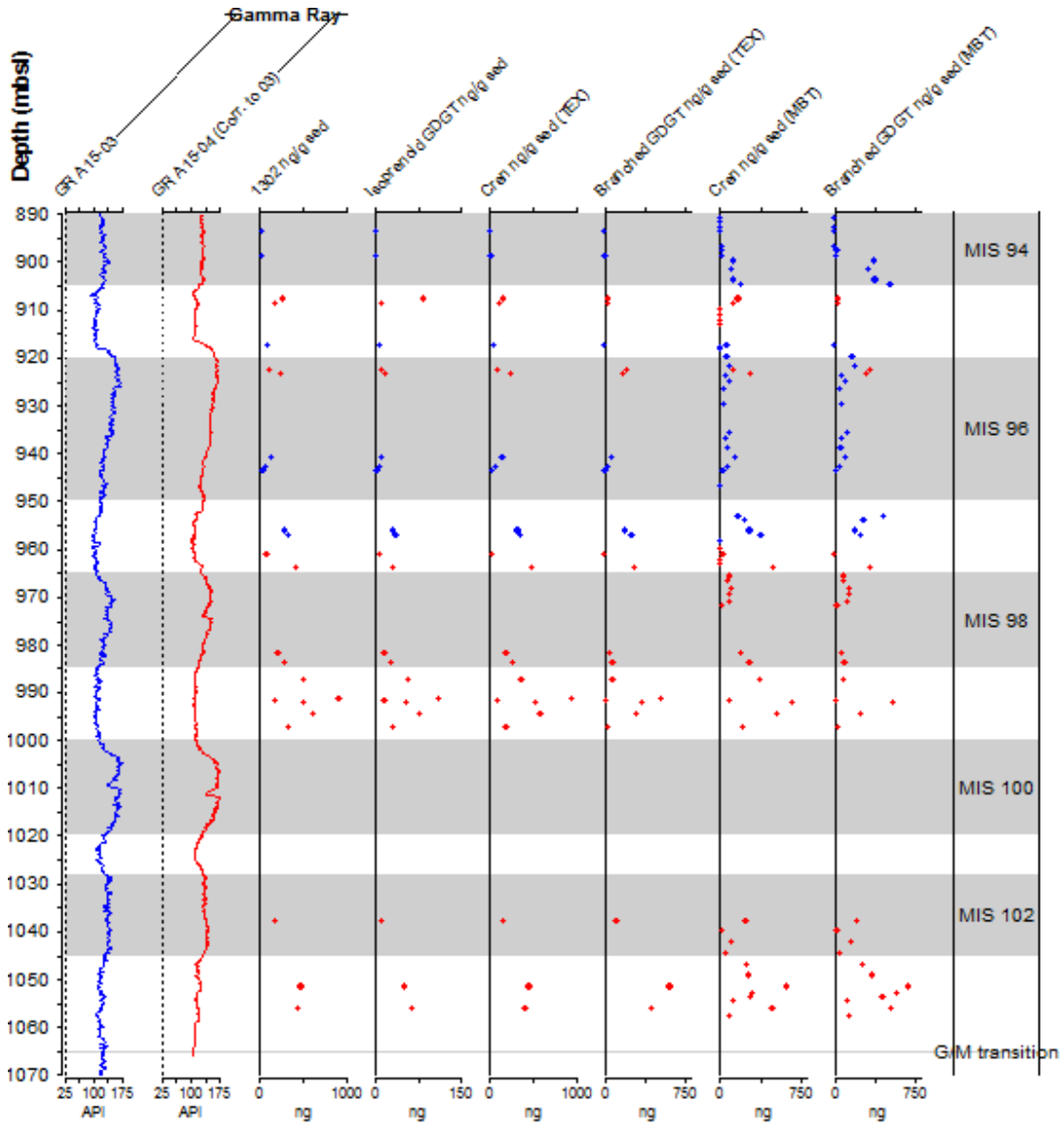

Figure 19) Diagram showing the relative abundances of GDGT-0 (1302), total isoprenoid GDGTs (except GDGT-0), Cren (both measured in the TEX and MBT method) and branched GDGTs (both measured in the TEX and MBT method). Blue represent samples from core A15-3 and red from A15-4.

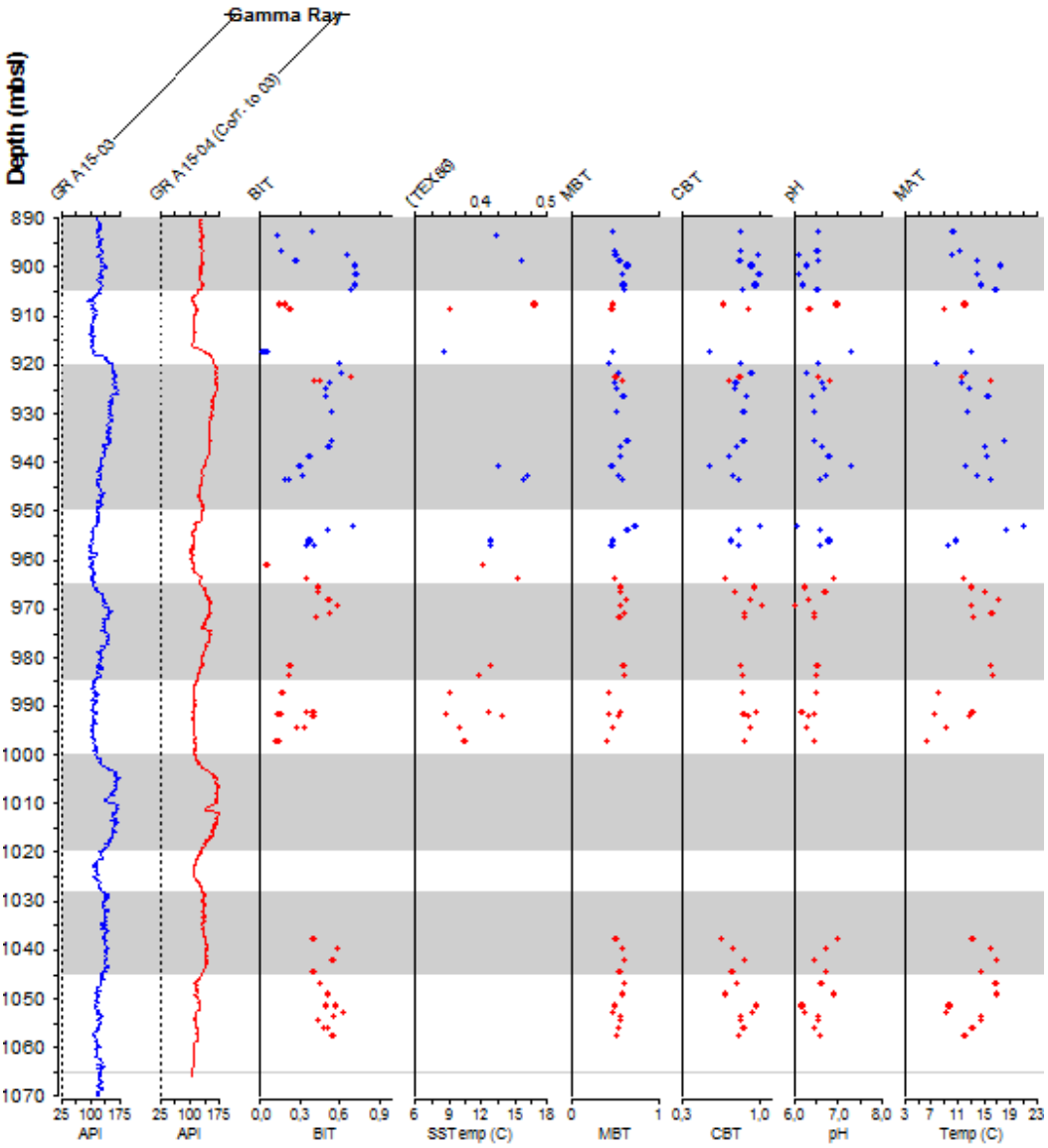

Figure 20) Diagram showing the BIT, TEX86, SST, MBT, CBT, pH and MAT data. Blue represent samples from core A15-3 and red from A15-4.

4.4 Oxygen and carbon isotopes

The benthic isotopic data (*fig.21*) are only available for a minor part of the section. This means that only MIS 98, 97, 95 and 94 are covered. The oxygen isotope record shows an enormous shift in the middle of MIS 98, going from values of +4‰ (V-PDB) to almost 0, and back to +4‰ again for the beginning of MIS 97. During MIS 97, the oxygen isotopes are quite stable, around 3‰. For MIS 95 the picture is similar, with a constant oxygen isotope signature around 2-3‰. Towards the transition zone from MIS 95 to MIS

94 the values switch towards heavier values of about 3.5‰. In MIS 94 the oxygen isotope values become increasingly heavier approaching 5‰. It is important to note that the trend in upper couplet is different from the trend in the lower couplet. Overall values (except the values for the shift in MIS 98) are in the range of the data presented by Zachos et al., (2008) and Lisiecki and Raymo (2005).

The carbon isotope record shows many similarities compared with the oxygen isotope record. Much scatter is observed in the middle of MIS 98, between +0.5‰ and -3‰. At the transition from MIS 98 to MIS 97 the values increase from -3‰ to -1‰ in the upper part of MIS 97.In MIS 95 values are rather constant, between -1 and -1.5‰. From the transition to MIS 94 onwards there is a decrease again to -3‰.

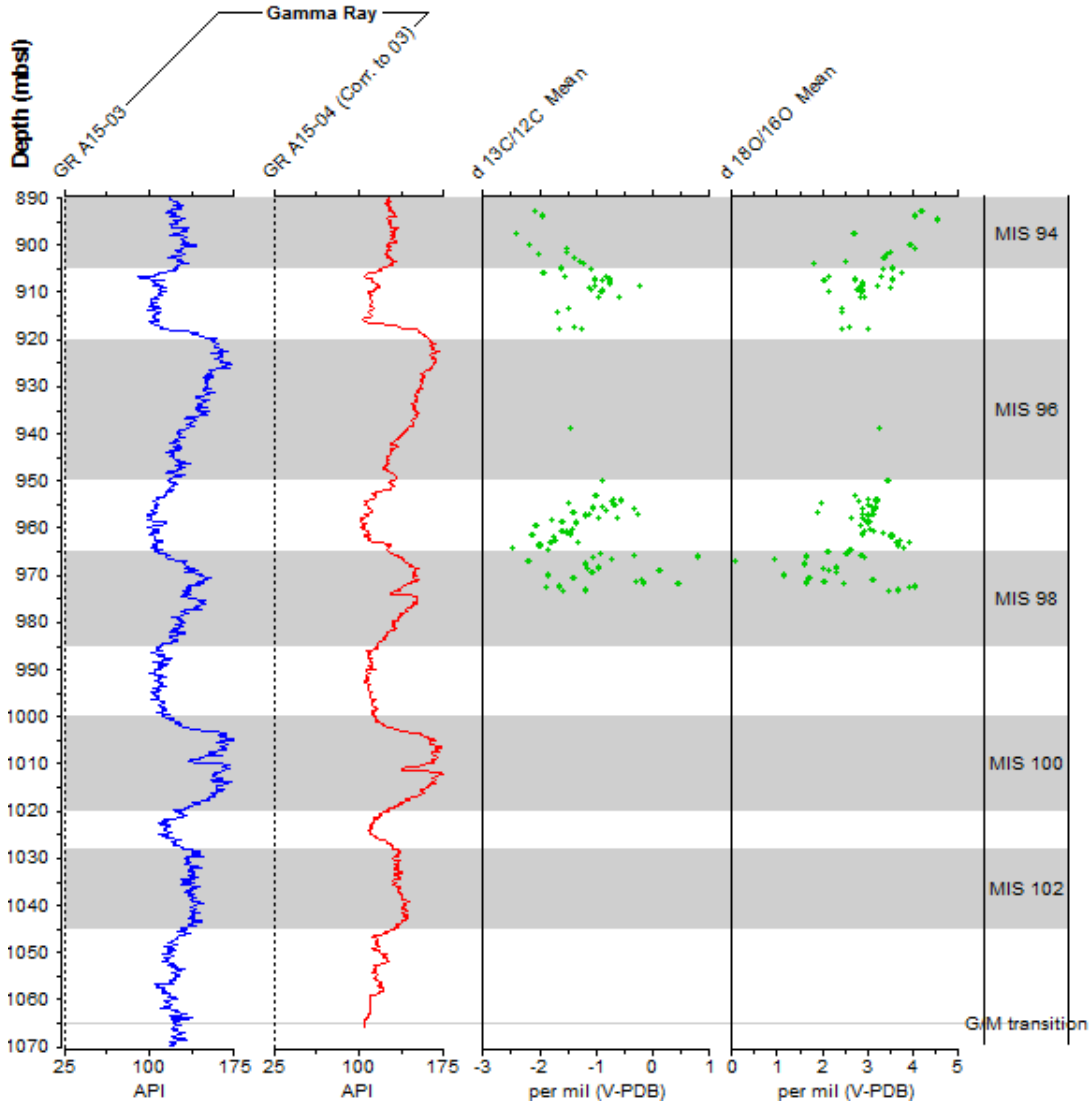

Figure 21) Diagram showing carbon and oxygen isotope data of the benthic foraminifer *Cassidulina teretis* throughout the record.

5 Discussion

5.1 Drainage area

As has become clear in chapter *2,* the studied sediments originate from a very large drainage area. The drainage area of the Eridanos river was about 1.100.000 km^2 (Overeem et al., 2001). Together with the drainage area of the Rhine-Meuse system (at present 221.000 km^2; van den Brink et al., 1993), we are dealing with a very large, and thus diverse source area. This means that climatologically speaking already large differences can be observed within the drainage area itself. *Table 2*, for example, gives an overview of present-day MAT observed throughout the source areas of the two river systems (*fig.22*) based on the world climate database of the Royal Dutch meteorological institute (KNMI). Present day MATs for the area once part of the Eridanos river system range between -0.5℃ and 8.7 ℃, with an average MAT around ~5.5℃. For the Rhine-Meuse area these temperatures are higher, ranging between 7.9℃ and 10.4℃, with an average around 9℃. This means a difference of ~3.5℃ in MAT between the two different drainage areas. Additional variation in temperature might have been present due to variations in altitude.

Although geography and climate of NW Europe were different during the Early Pleistocene it is, thus, important to take into account that variations observed in our records might not only represent absolute differences in Early Pleistocene climate but that they, at least partly, could also be a result of changes in drainage area within this large river catchment. This is likely an explanation for part of the higher order variation that is observed throughout the different records. General trends in the palaeoclimate records are, however, supposed to be reliable. This is supported by the fact that (terrestrial) climate trends obtained from pollen records and organic geochemical records show clear similarities with climate trends based on dinocyst assemblages (Kuhlmann et al., 2006). Whereas pollen and land-derived biomarkers might depend on source area, dinocyst assemblages do depend on the amount of river discharge but are independent of drainage area.

Nr.	City/Country	MAT (°C)	Nr.	City/Country	MAT (°C)
1	Kuusamo/Finland	-0.5	11	Gdansk/Poland	7.5
2	Jokkmokk/Sweden	-0.4	12	Kopenhagen/Denmark	8.0
3	Stockholm/Sweden	6.6	13	Hamburg/Germany	8.7
4	Helsinki/Finland	4.5	14	De Bilt/Netherlands	9.4
5	Tallinn/Estonia	5.1	15	Cologne/Germany	10.4
6	Kalmar/Sweden	7.3	16	Frankfurt/Germany	9.5
7	Riga/Latvia	6.2	17	Luxembourg(City)	8.3
8	St. Petersburg/Russia	5.0	18	Nancy/France	9.4
9	Vilnius/Lithuania	6.0	19	Karslruhe/Germany	10.3
10	Warschau/Poland	7.8	20	Zurich/Switzerland	7.9

Table 2) Present-day mean annual air temperatures of climate stations situated in the ancient drainage area of the Eridanos River (black) and the Rhine-Meuse drainage area (grey). The locations of the climate stations are given in *figure 21*. MATs were obtained from the World Climate Information database (KNMI, 1997) of the Royal Dutch Meteorological Institute (KNMI) and represent a 30 year average over the period 1961-1990.

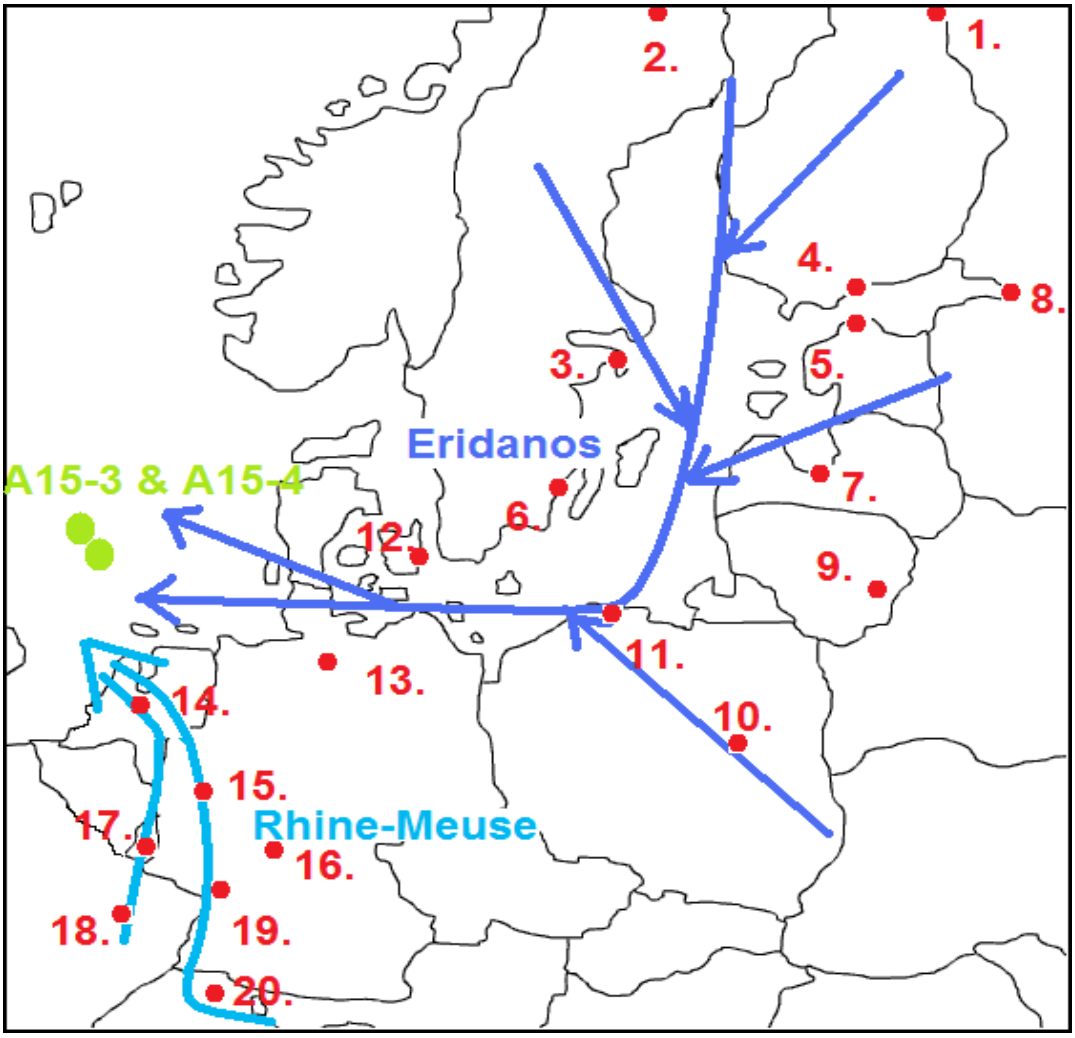

Figure 22) Locations of the climate stations situated in the ancient Eridanos drainage area and the present-day Rhine-Meuse drainage area.

5.2 Terrestrial OM input and sea level variations

The records for TOC and the C/N-ratio (*fig.14*) show the best correlation with lithology. Trends in the abundance of alkenones, *n*-alkanes (*fig.16*) and GDGTs (*fig.19*) also have a lot in common with lithology.

For the coarser-grained intervals, TOC values (*fig.23*) are higher than for the clay intervals. Alkenones, *n*-alkanes and GDGTs also show peak abundances in or around the coarser intervals. Higher C/N ratios also occur in the coarser intervals. According to the Redfield-ratio (Redfield, 1934), C/N ratios of marine primary production and thus of marine derived organic matter are more or less constant around 106/16 (~6.6). For the coarser intervals these values are doubled or almost tripled (*fig.23*), suggesting a dominant terrestrial source for the organic material. For the clay intervals the C/N ratios are still above 6.6, however, values of 8 indicate that, relative to the coarse intervals, a larger part of the organic matter consists of marine derived organic matter. The clay interval representing MIS 96 is the only interval of the section where values drop below the Redfield-ratio (~3.5).

Throughout the record ACL (*fig.23*) varies between ~29.3-29.8. According to Jeng (2006) this suggests that the long chain *n*-alkanes are mainly land derived. *n*-Alkanes of marine origin have much lower chain lengths (C_{16}-C_{24}). The values found here, thus, indicate an almost pure terrestrial source. It has to be mentioned that *n*-alkanes can be transported efficiently from land to sea by both rivers and wind, which might, at least partly, explain the dominance of long chain *n*-alkanes. The lowest values found in this study appear in the clay intervals (the absolute minimum (~29.3) is located in MIS 96), pointing to a slightly higher marine input relative to the coarser grained intervals.

CPI (*fig.23*) varies between ~2.8-4.5, suggesting leaf waxes of terrestrial plants to be the main source for *n*-alkanes in the sediments (Jeng, 2006), which is a confirmation of the signal shown by ACL. However there is also some marine influence, playing a larger role during the CPI minima around the transitions from the coarse intervals to the clay intervals.

Overall, the BIT index (*fig.23*) is showing values (~0.55 on average) reflecting a considerable input of terrestrial derived OM. Low BIT values are mainly appearing in the coarser grained intervals and the start of the clay intervals, highest BIT values are found in the clay intervals. Since branched GDGTs are almost exclusively transported by rivers (rather than by wind), the BIT index not only represents absolute differences in soil

organic matter supply, but also relative differences due to sea level fluctuations. During periods with a higher sea level, as a result of a warmer climate (decreased storage of sea water in icecaps), the core sites were located relatively further offshore. Therefore relatively less terrestrial OM arrived at the core sites during this periods, reflected in a BIT signal pointing to a predominant marine source of GDGTs.

Based on a high C/N ratio, high ACLs, high CPI values and a high BIT index, it is concluded that the majority of the OM present in the studied section is derived from a terrestrial source. Obviously, this is not unexpected in a river fan which resembles in size the current Indus Fan (McHargue and Webb, 1986; Kolla and Coumes, 1987). During MIS 96 the C/N-ratio drops far below the Redfield-ratio (~3.5), a minimum in ACL is also reached during this period, these findings both point to a relative increase in marine derived organic matter. An absolute minimum in TOC values is also observed in MIS 96, therefore this part of the record can be seen as the interval with the lowest input of (terrestrial) organic matter. This low runoff may be the result of drier conditions on the continent (i.e. less vegetation, soil formation and river runoff), larger permafrost areas and build up of glaciers on the Fennoscandian Shield (though small compared to the size of the catchment area), or a combination of the three. This hypothesis is also supported by the low water transported pollen counts (all pollen except *Pinus* and *Picea*; *fig.11*) for this interval, suggesting very harsh conditions (e.g. a polar desert). However from the pollen records we also observe an increased occurrence of *Pediastrum* (a freshwater algae). Increased *Pediastrum* occurrences might be the result of enhanced river runoff, which would contradict the hypothesis for less freshwater influx. On the other hand enhanced *Pediastrum* occurrences might also be the result of an increased number of ponds and lakes, as a result of extensive wetlands and swamps.

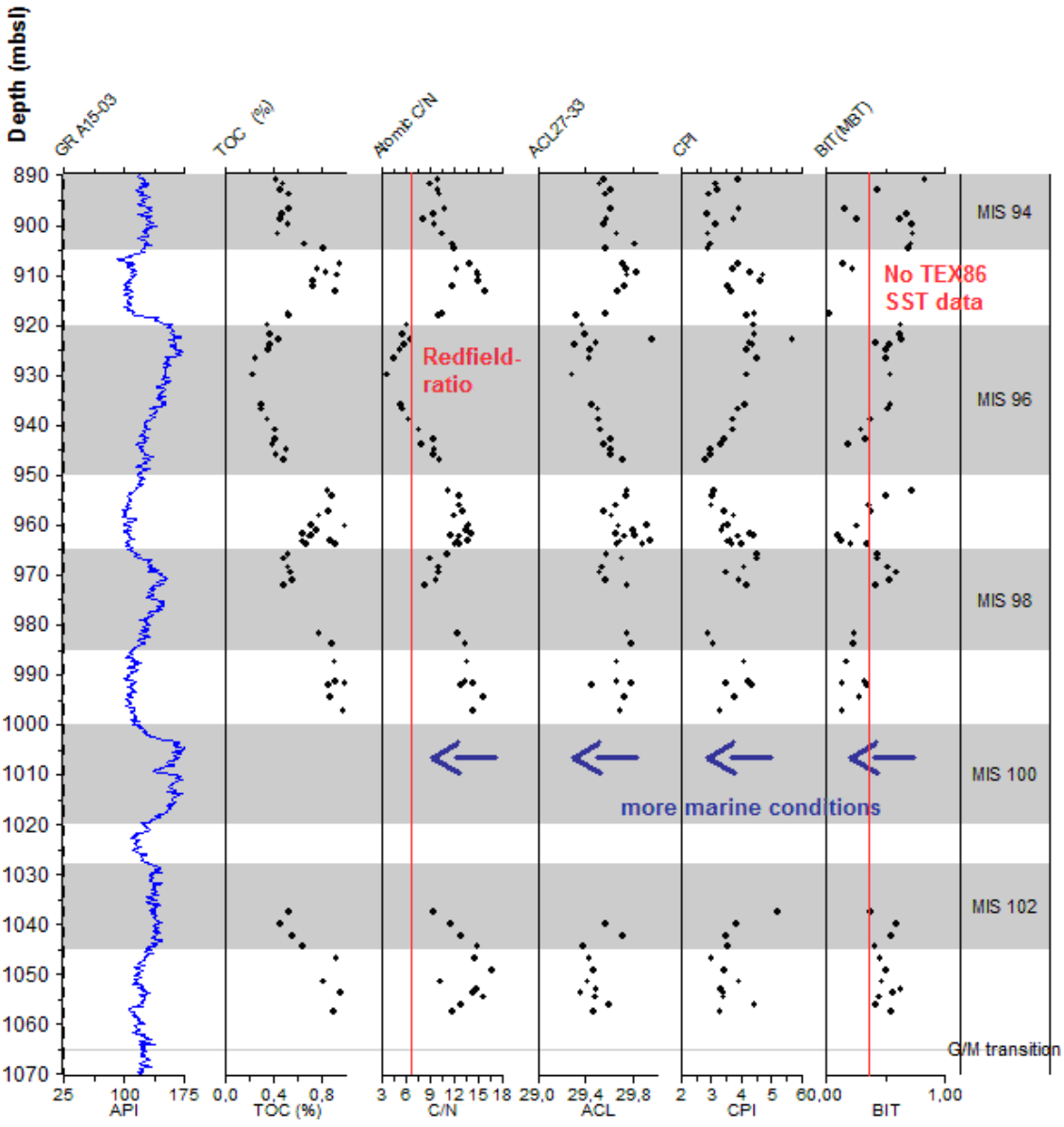

Figure 23) An overview of the data discussed in section *5.2*. With lines and arrows indicating important environmental parameters.

The higher TOC values in the coarser intervals might be caused by an increase in vegetation and soil formation, an increased terrestrial runoff, an influx of thawing permafrost soils or a combination of the discussed options. All options reflect a (change to) warmer climate with more humid conditions. Although terrestrial organic matter is dominant throughout the section, there might also be an enhanced input of marine organic matter during these coarser grained intervals. Minima in CPI occur around the transitions from the coarse intervals to the clay intervals. BIT data support this trend,

showing lower values (thus a relatively larger input of marine derived isoprenoid GDGTs) in the coarser intervals. Based on CPI and BIT data it may be concluded that the contribution of marine organic matter was higher around the transitions from the coarser intervals to the clay intervals. This contradicts the findings for the C/N ratio and ACL, discussed previously in this section. This increase in marine organic matter contribution may be related to a higher sea level, which fits with the reconstructed SST and MAT data (section *4.2.4*) showing maxima around these transitions, allowing relatively high sea levels.

Oxygen isotope compositions of benthic foraminifera (*fig.21*), although more difficult to interpret due to scattering and likely overprinted by freshwater input, partly support the CPI and BIT data. Although scatter is large (around 2‰), the clay interval correlated to MIS 94 shows an average increase of about +1.5‰ relative to the adjacent coarser grained interval correlated to MIS 95. Such an increase is comparable in magnitude with the increase in $\delta^{18}O$ found by Sosdian and Rosenthal (2009) for the North Atlantic, which was attributed to the development of ice sheets in the Northern Hemisphere during the Early Pleistocene. When the large isotopic excursion (which might be caused by salinity changes, stratification or regional climate variability) in the upper part of the clay interval correlated to MIS 98 is ignored, a decrease from values around +4‰ to +2.5‰ is found for the transition to the coarser grained interval correlated to MIS 97. Such an isotope shift is comparable in size (though the other way around; -1.5‰) with the one observed for the transition from MIS 95 to MIS 94, which might be related to an increase in ice volume. For the transition from MIS 98 to MIS 97 this would mean a decrease in ice volume. During the coarser intervals MIS 97 and MIS 95 oxygen isotope compositions are similar and rather stable. The similarity between these two MISs is probably the result of similar climatic conditions during these stages, e.g. similar SSTs and ice volume. $\Delta^{18}O$ values for these intervals are closer to 0 compared to values for the adjacent clay intervals. This would imply that MIS 97 and 95 represent periods with less or no icecaps and thus a higher sea level. Unfortunately MIS 96 is not covered because of a lack of benthic foraminifera. This might be the result of dissolution (Kuhlmann et al., 2006) or stratification and salinity changes induced by the glacial-interglacial cycles.

5.3 Marine climate

5.3.1 Palynology

Marine climate changes around the Pliocene-Pleistocene transition in NW Europe have been analyzed using both dinocyst assemblages and geochemical biomarkers. During the Pliocene the warm species of *Operculodinium israelianum* is still highly abundant (Kuhlmann et al., 2006). After the Pliocene-Pleistocene transition a sharp decline in their (relative) abundance was observed, and a sharp increase in cold-adapted species (i.e. "cool taxa") was reported (Kuhlmann et al., 2006), i.e. *Brigantedinium* spp., specimens of the *Habibacysta*/*Filisphaera* group and *Bitectatodinium tepikiense*. This increase in cool taxa is an indication for lower seawater temperatures, which most likely is related to a shift towards a colder climate in general. Based on results from previous studies (Kuhlmann 2004; Kuhlmann et al., 2006), in combination with the dinocyst assemblages analysed in this study, it has become clear that for the studied sections in the Early Pleistocene the clay intervals are mainly dominated by cold-indicating dinocyst assemblages. The coarser grained intervals are a mixture of cold-indicating species with some punctuations by warm-indicating species, i.e. *Operculodinium israelianum*. All together it is concluded from the dinocyst assemblages that seawater temperatures drop after the Pliocene-Pleistocene transition. During the Early Pleistocene marine climate fluctuates, with warmer conditions reconstructed for the coarse intervals and colder conditions reconstructed for the clay intervals.

5.3.2 Temperature reconstruction

The reconstructed UK'_{37} SSTs are much higher than TEX_{86} reconstructed SSTs. The absolute values for SST reconstructed with the UK'_{37} index are with 16°C to 25°C unrealistically high given oxygen isotope compositions of deep sea benthic foraminifera for the same period (e.g. Lisiecki and Raymo, 2005). In fact, the UK'_{37} SSTs and abundances of the ketones in ng/g dws follow the trends observed in the gamma ray logs. This could indicate that their occurrence is strongly influenced by fluvial dynamics. For example (part of) the alkenones may have been produced by haptophyte algae living in freshwater environments, which afterwards have been transported to the studied sites by the Eridanos river. Alkenones synthesized by fresh water algae might have a different or no correlation at all towards temperature in contrast to alkenones produced by marine pelagic algae (Toney et al., 2010), and thus bias the reconstructed SSTs. Along similar lines, large freshwater input at this site could have resulted in more brackish conditions and thus a different species of algae. In general, it has to be mentioned that the species

of alkenone synthesizing haptophyte algae that are used for calibration of the UK'_{37} (*Emiliania huxleyi* and *Gephyrocapsa oceanica*; e.g. Prahl and Wakeham, 1987; Volkman et al., 1995) did not yet exist at the Pliocene-Pleistocene boundary. So it is unknown if species existing around that time have a similar calibration towards temperature. Given all this, the UK'_{37} reconstructed SSTs are not considered reliable.
As discussed in section *4.2.4*, based on the BIT index, samples with too high input of terrestrial derived isoprenoid GDGTs have been omitted. Therefore, the TEX_{86} derived SST reconstructions presented here are expected to represent reliable SST reconstructions for the Early Pleistocene in NW Europe. Compared to the UK'_{37} SST reconstructions, the TEX_{86} SST reconstructions show more realistic values (between 9°C and 17°C). This means that the amplitude of SST variation is about 8°C, which is comparable with the reconstructed amplitude based on shifts of 1.5‰ in the oxygen isotope composition of benthic foraminifera between the coarse and clay intervals, which translates to an amplitude of ~6.5°C (Ruddiman, 2001). Furthermore the amplitude of SST changes seems to fit with the expected amplitude, based on a previous study by Bintanja and Van de Wal (2008). In the study of Bintanja and Van de Wal (2008) an amplitude of about 12°C was modelled for the surface air temperature of North America around the Pliocene-Pleistocene transition. Keeping the heat capacity of water in mind the observed ~8°C amplitude in SST of this study fits with the outcomes of that previous study. The SST change of ~8°C reconstructed here between glacials and interglacials is similar to SST changes reconstructed using UK'_{37} for the last deglaciation in the Northeast Atlantic (Zhao et al., 1993), this implies that Early Pleistocene glaciations (with a 41ky cyclicty) show similar magnitudes as those of the Late Pleistocene (with 100ky cyclicity).

5.4 Terrestrial climate

5.4.1 Palynology

Terrestrial climate evolution around the Pliocene-Pleistocene transition in NW Europe has been analyzed using both palynology and geochemical biomarkers.
For the pollen, the disappearance of *Taxodium* in the middle of MIS 102 (*fig.12*) is noticeable. Based on the ecology of *Taxodium* (Farjon, 2005) the disappearance of this species might be related to an intensification of winter conditions (i.e. more severe

winters). A similar trend (sharp decline in the warmer *Operculodinium israelianum* species) was observed in the dinocyst assemblages, discussed in section *5.3.1*. Although lithology and palynology do not show a perfect phase relation, an obvious trend can be observed in the pollen records from the disappearance of *Taxodium* onwards. The coarser grained intervals are dominated by pollen indicative of warm conditions. The clay intervals are mainly dominated by cold-indicating pollen like *Ericaceae* and *Sphagnum*. Based on the C_{23} *n*-alkane abundances (indicative for *Sphagnum* species; Nichols et al., 2006) the same conclusion can be drawn, with relatively high C_{23} abundances in the clay intervals.

5.4.2 Temperature reconstruction

Throughout the record there is a lot of scatter in the reconstructed MAT data. This scatter may be related to the application of the MBT/CBT proxies. Despite the promising results, these proxies have only been empirically established and some uncertainty exists over their calibration and the impact of other environmental factors (Peterse et al., 2009). The poor resolution of the peaks in the HPLC-MS chromatograms (discussed in section *4.2.4*), may cause part of the scatter. Though absolute temperature estimates may suffer from this, trends in MAT estimates will nevertheless be reliable. Theoratically, the observed scatter might also be a result of large and very rapid changes in drainage area, although no evidence for such dramatic changes in drainage area exists. The MATs reconstructed with the MBT/CBT proxy show temperatures for MIS 103/102, (the last interval with *Taxodium* occurrences), between ~9°C and ~17°C. These temperatures are in accordance with temperatures reconstructed by Donders et al., (2009a) for the Pliocene, which range between ~11°C and ~16°C. From MIS 99 onwards a clear trend is observed in the MAT estimates. The reconstructed MATs, show, similar to the pollen records, alternating intervals of warming and cooling, schematically presented in *figure 24*. The amplitude of the reconstructed MAT is in accordance with the amplitude of up to 12°C in surface air temperatures modelled by Bintanja and Van de Wal (2008) for North America in the same period. These amplitudes in temperature are similar to the amplitude for the last glacial-interglacial transition, as recorded by air trapped in polar ice (Severinghaus and Brook, 1999). Although the first Northern Hemisphere glacial cycles appear during the Early Pleistocene, only minima in MAT during the Early Pleistocene are lower than today's MAT. This contradicts the findings of Bintanja and

Van de Wal (2008) for North America with reconstructed surface air temperatures up to 11°C cooler compared to present day temperatures. The lower temperature estimates for North America might, at least partly, be the result of the landmass configuration for North America, leading to a different climate regime (dry) compared to NW Europe (temperate). On the other hand, the influence of the warm Gulf Stream on NW Europe might have resulted in a tempering of the drop in annual MAT in NW Europe. Finally, it has to be noted that the temperature maxima reconstructed here for NW Europe are surprisingly high, i.e. up to 21°C. Certainly if taken into account the source of the majority of the sediments, and thus of the OM including the GDGTs, i.e. originating from the Fennoscandian shield (*fig.7*). These maximum MATs are comparable with average MATs reconstructed for the Late Miocene for NW Europe (Donders et al., 2009). As discussed, absolute MAT reconstructions are associated with a standard error of estimate of ca. 5.5°C, which might account for part of the high value. Given that all reconstructions here are derived from the same place, the trend in annual MAT reconstructions is, nevertheless, supposed to be reliable.

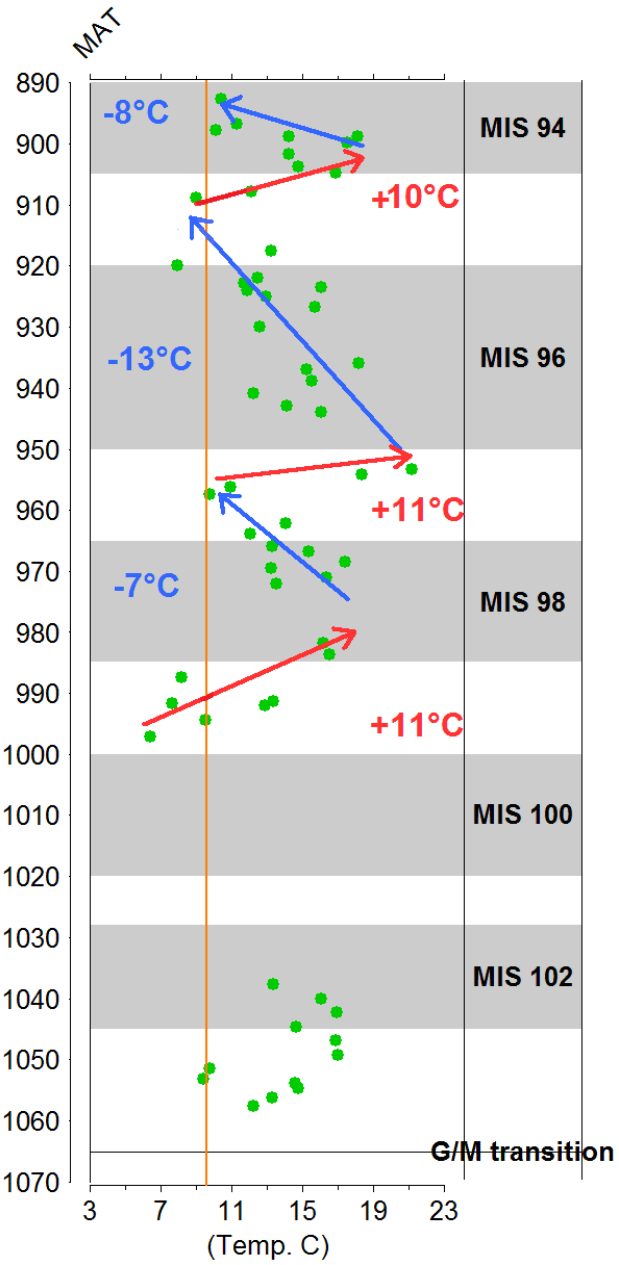

Figure 24) MAT reconstructions based on branched GDGT proxies (MBT+CBT). In green are the data points of both core A15-3 and A15-4, with help of red and blue arrows temperature trends are indicated. The orange line indicates MAT (~9.5°C) for the Netherlands in the period1961-1990. Furthermore the lithology (clay intervals grey, coarser intervals white) and different MIS are added.

5.4.3 Time lag

From an overview of all the data it has become clear that there is a large difference in phasing between the warm and cool intervals deducted from the pollen and dinocyst records and reconstructed with the MBT/CBT proxy. This might be the result of large amounts of sediment that are released from glaciated and frozen soils and deposited during the start of a deglaciation. The coarse facies and low palynological yield suggest rapid sedimentation. These rapidly deposited sediments might still contain old GDGTs from glacial soils reflecting a much colder signal. This might also be an explanation for the large amplitude in MAT reconstructions. The sudden pulses of the previous glaciated soils result in temperature signals which are much cooler than the average temperature signal for the catchment area.

It is hard to determine the size of the time lag. Because the glacial cycli in the Pleistocene, until the Mid-Pleistocene-Transition, are governed by obliquity, an even and an odd MIS together must represent about 41 ky . Furthermore Kuhlmann et al. (2006) determined the sedimentation rate for this section, which lies most likely between 78 and 84 cm/ky. Unfortunately the sedimentation rates for the individual parts of the sections (i.e. clay and coarser grained intervals) are not known. From the data it is observed that the lag is in the order of ~5 to 10 meters, which would mean that we are dealing with at time lag of at least a couple of thousands of years. But when the sedimentation rate for the coarser grained intervals was much higher, i.e. 5-10 meters/ky, we are dealing with a maximum time lag of just one thousand year.

5.5. Identification of marine isotope stages in the Early Pleistocene

The different proxies used in this study almost all show strong alternations coupled to the first 41 ky glacial-interglacial cycles in the Northern Hemisphere (*fig.25*). Although the proxies show similar alternations, they do not all show the same phasing, e.g. reconstructed MAT versus palynology (section *5.4.3*). The stratigraphic model of the cores used in this study relies on magnetic susceptibility and gamma ray logs to identify the lithology, which consists of clay and coarser grained (silt to sand) units. Subsequently the clay intervals were tentatively correlated to the even Marine Isotope Stages (glacials) and the coarser grained intervals to the odd Marine Isotope Stages (interglacials), based on palynology. However, part of the organic geochemical proxies

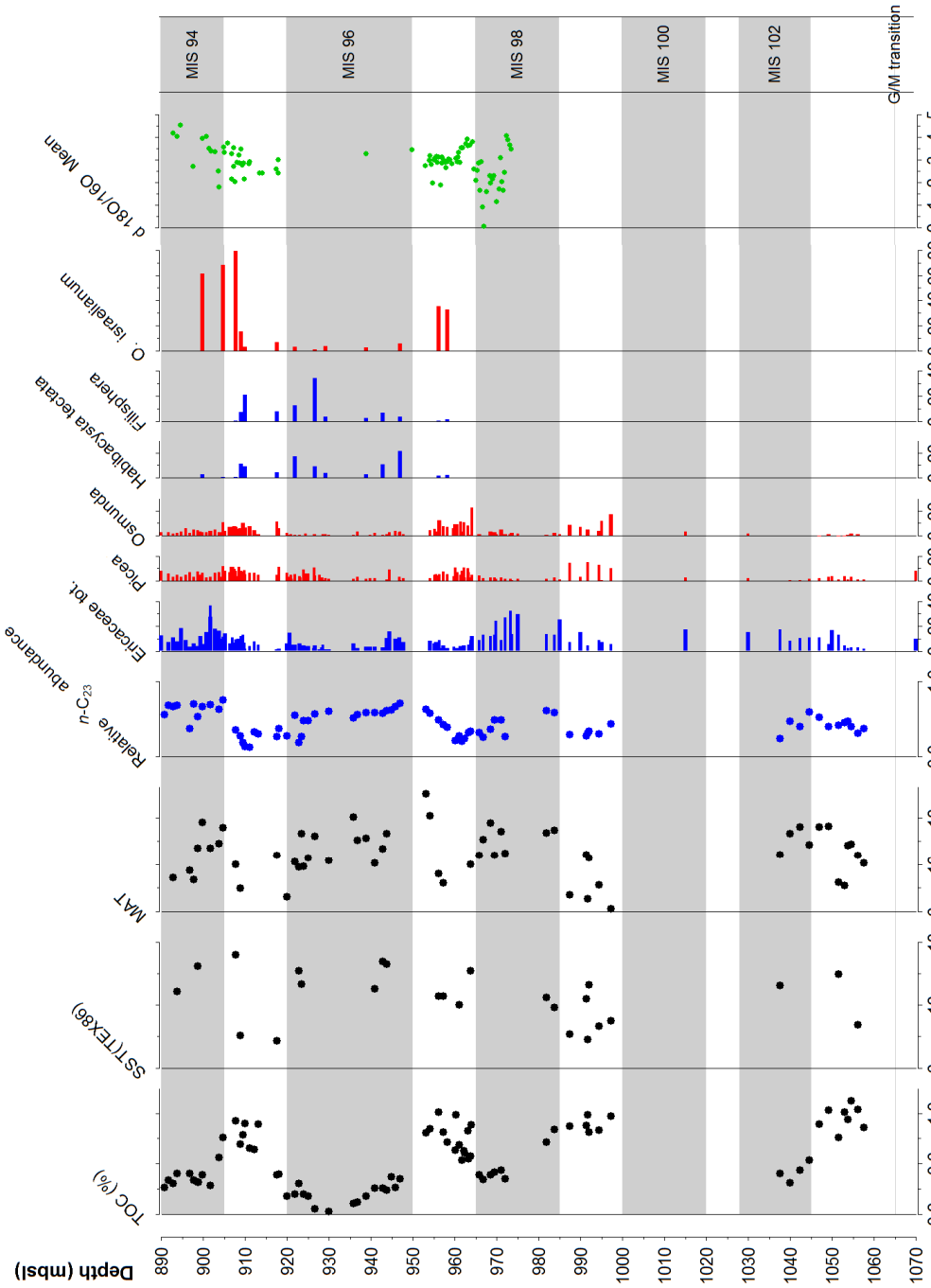

Figure 25) Overview of the most important proxy data (both palynology and geochemistry). "Warm taxa" are plotted in red and "cool taxa" are plotted in blue. Relative *n*-C_{23} abundance is plotted in blue, as higher *n*-C_{23} values are indicating higher abundances of *Sphagnum*, which is indicative for colder periods.

tend to point to a correlation that should be the other way around, i.e. clay units should represent warm phases (interglacials; odd MIS) and the coarse sand units the cold phases (glacial; even MIS). In fact, based on basic sedimentology we would also expect clay to be deposited during interglacial stages as it goes together with a transgressive systems tract. During a transgression sea level rises and the studied sites would have been located relatively further offshore, which means less energy to transport particles,

thus sedimentation of the finer (clay) fraction. The coarser fraction would be linked to a glacial stage, which is characterized by a regressive systems tract. During a regression sea level falls and the studied locations would have been located closer to the shore, which means more energy to transport particles, thus deposition of coarser (heavier) particles at the studied sites. This new hypothesis of clay deposition during sea level high stands, i.e. interglacials, (*table 3*) is clearly supported by the C/N ratio and the ACL, which both indicate more marine organic matter input in the clay intervals and higher terrestrial organic matter input in the coarse grained intervals. Furthermore the MBT/CBT reconstructed MATs show minima in the coarser grained intervals, similar to the TEX_{86} derived SSTs, thus both indicating coolest conditions during deposition of the coarse grained intervals.

Proxy	Glacials represented by the clay intervals	Glacials represented by the coarser grained intervals
Lithology		X
Pollen records	X	
Dinocyst assemblages	X	
C/N ratio		X
CPI	X	
ACL		X
BIT	X	
TEX_{86} SSTs		X
MBT/CBT MATs		X

Table 3) The different proxies indicating the different correlation between the used proxies

However CPI and BIT values are indicating enhanced marine organic matter input in the coarser intervals, as discussed in section *5.2*. Although this seems contradicting with the new hypothesis, the low BIT data in the coarse sediments might be a result of differences in preservation of the GDGTs between the two lithologies, i.e. GDGTs are likely dominantly transported associated to clay particles and likely better protected by clay particles then by a coarser mineral matrix. The CPI is generally high reflecting continuous high input of terrestrial organic matter. In fact the CPI is also commonly used as maturity indicator. Due to differences in preservation the CPI could be slightly lower in coarser grained sediments and higher in the clay intervals. Although oxygen isotope compositions of benthic foraminifera tend to support the “classical” identification of the Marine Isotope Stages, scattering and the likely overprinting by fresh water makes them complicated to interpret and link to MIS identification.

From a summary of all the different proxy data it may be concluded that the coupling of the studied record to the glacial-interglacial cycles, represented by MIS 103-94, is a lot more complicated than thought before. The complicated coupling of the MIS 103-94 to this record might lay in the provenance of the sediments. Based on extensive sedimentary studies Westerhoff (2009) concluded that the Rhine-Meuse system was predominantly depositing sediments in the Southern part of the North Sea basin during the Early Pleistocene. Although there is evidence for several periods during the Early Pleistocene in which the Rhine-Meuse system merged with the Eridanos system, the much larger sediment supply of the Eridanos system dominated sediment deposition at the studied sites. Kuhlmann (2004), on the contrary, concluded, based on mineralogical data, that the sediments deposited in the central North Sea Basin during the Early Pleistocene were derived from two main sources. The finer clay mainly originated from the Fennoscandian Shield (*fig.6*) and was transported over long-distance by the Eridanos river. Coarser, smectite-rich, sediments mainly originated from proximal volcanic areas to the south, drained by the Rhine-Meuse river system.

Thus, the identification of two different main sources for the sediments deposited in the clay and coarse grained interval might provide an explanation for the contradicting pollen results (compared to the geochemical proxy results). During low sea level stands (usually more glacial conditions), when the coarse grained fraction was deposited, the sediments, and thus also the pollen, are for a large part derived from the more southern locations in the catchment area. Therefore the coarser grained sediments might show a relatively warm vegetation signal. On the contrary, during high sea level stands, sediments, and thus also the pollen, are predominantly derived from the northern Fennoscandian Shield, reflecting a relatively cool signal. As for the dinocysts, reworking of the fossil assemblage might be an explanation for contradicting dinocyst results. It is very well possible that during a sea level regression the warm dinocyst species deposited in lagoons during sea level high stand (interglacial), were reworked by the prograding river(delta) and redeposited at the core locations (Brinkhuis, pers. comm.) thereby overprinting the actual climate signal.

Based on these data and explanations it is proposed to change the annotation of Marine Isotope Stages in such a way that the clay intervals represent the interglacials and vice versa.

6 Conclusion

Overall, both palynological and organic geochemical proxy records show surprisingly strong alternations of warmer and cooler intervals, which can be coupled to the first 41 ky glacial-interglacial cycles for the Early Pleistocene in NW Europe. Both marine and terrestrial records are generally in phase with each other. Therefore it is concluded that there was a strong climate coupling of marine and terrestrial environments.

The petrochemical proxies based on the distribution of long chain *n*-alkanes, in combination with the C/N ratio and the BIT index, provide evidence for a predominant terrestrial source of organic matter in the sediments of the central North Sea Basin at this time. All proxy records, however, show episodes with enhanced input of marine derived organic matter coupled to sea level variations as a result of the glacial-interglacial cycles.

In the first clay interval after the Pliocene-Pleistocene transition *Taxodium* has its last occurrence as a result of intensified winter conditions. Although lithology and palynology do not show a perfect phase relation, an obvious trend is observed. From the disappearance of *Taxodium* onwards, the clay intervals are dominated by cold-indicating pollen like Ericaceae and *Sphagnum*. Dinocyst assemblages are also dominated by "cool taxa" in the clay intervals. The coarser-grained intervals are mainly dominated by pollen and dinocysts indicative for warmer conditions, e.g. *Osmunda* and *Operculodinium israelianum*.

Both isoprenoid and branched GDGTs are present in the studied sediments. MAT estimates based on the MBT/CBT proxy show for the first coarse and clay interval after the Pliocene-Pleistocene transition temperatures comparable to temperatures earlier reconstructed for the Pliocene. For the upper part of the studied section a glacial-interglacial pattern is observed. Lower MATs, with minima around 6 to 9°C, are reconstructed for the coarser intervals, while higher MATs, with maxima varying between 17 and 21°C, are reconstructed for the clay intervals. Unfortunately only a minor part of the samples was suited for the application of the TEX_{86}-proxy, due to high input of terrestrial organic matter. Trends in reconstructed SST based on this proxy are, nevertheless, comparable with trends in reconstructed MAT. Low SSTs are reconstructed for the coarser grained intervals, with minima around 9°C. SSTs reconstructed for the coarser grained intervals are higher, with maxima up to 17°C. Long chain alkenones were present as well in some samples, but SST reconstructions based

on their distribution (UK'_{37} proxy) do not reflect realistic values. This might be due to the presence of fresh water tolerant species of the source organism, biasing the alkenone distribution. The amplitude of the reconstructed MATs and SSTs is comparable with results from previous studies. Absolute temperatures during the first glacial-interglacial cycles are, nevertheless, higher than expected for the Early Pleistocene of NW Europe.

The initial correlation of lithological units to Marine Isotope Stages is based on trends in the pollen and dinocyst composition, i.e. “warm” assemblages in the coarser grained intervals and “cool” assemblages in the clay intervals. Trends in the paleotemperature reconstructions, however, are mirroring these palynological records, and therefore contradict the previously established correlation. Previous studies to the mineral composition of the sediments making up the two lithological units suggest different provenance areas for both. This, in combination with reworking of sediments by deltaic and fluvial dynamics, provide a potential explanation for the contradicting records. This would imply that the clay intervals represent the warmer interglacial stages and the coarse-grained intervals represent the cooler glacial stages.

7 Further research

Based on the material studied here, the organic geochemical potential of the samples could be further explored. For example, hopanes and steranes might be identified in the apolar fractions. The polar fractions have, unfortunately, not been studied at all yet with respect to the GC amenable proxies. Biomarkers that might be encountered include alkanols, hopanols and sterols (e.g. dinosterol derived from dynoflagellates). It has to be acknowledged though, that based on the results of the apolar fraction, the amounts of these biomarkers are likely to be low, especially in the polar fraction as, over time, due to diagenesis reactions functional groups tend to get lost.

The sediments used in this study primarily originate from NW Europe, therefore we can only reconstruct the climate evolution for NW Europe in this study. To get a better grip on global climate evolution around the Pliocene-Pleistocene boundary and the Early Pleistocene, more high resolution multi-proxy studies are needed, based on sediments originated from other areas. It is particularly interesting to study the climate evolution in polar regions, from which it is known that they are highly sensitive to global climate change. Furthermore, it is also interesting to study how climate evolved in low latitude areas during this time interval and to see how the meridional temperature gradient developed over this important boundary as that gradient seems to be the result of global circulation patterns.

It would also be interesting to focus on one climate cycle in even more detail (e.g. MIS 96 and MIS 97), to better understand the phase relationships between temperature and other indicators for environmental change such as oxygen isotopes, carbon isotopes and proxies for sea level change. This might help to further unravel the forcing mechanisms. This might also provide an explanation for the high order variation within single intervals as observed in this study. Furthermore it might be possible to identify (if present) short term climate variability, i.e. events similar to the Heinrich events and Dansgaard-Oeschger events.

Acknowledgements

This research project had not been possible without the help of many people. Hereby I would like to thank these persons for their contributions.

Gert-Jan Reichart is thanked for offering the chance to participate in this project. Wintershall Noordzee B.V. and TNO are thanked for providing the offshore samples used in this study.
I am grateful for the help of my GeoBio colleagues at TNO B&O. Many people supported me during my palynological expedition and with the interpretation of data: Frans Bunnik, Dirk Munsterman, Roel Verreusel, Heleen Koolmees, Marianne and Susan.
I also want to thank my colleagues of the Organic Geochemistry group at Utrecht University, they provided literature, helped me with organic geochemical lab work, involving measuring on the GC and GCMS and interpretation of data: Klaas Nierop, Laura Buckles, Mohamed Elkelani, Cornelia Blaga, Els van Soelen, Julia van Winden, Anita van Leeuwen and Jan Kubiak.
Lucas Lourens is acknowledged for his advise in the interpretation of the isotope-data. Jan Drenth for freeze drying and crushing of the samples. Dineke van de Meent for her help with the decalcification of the samples for TOC analysis. Arnold van Dijk for measuring TOC and benthic isotopes. Jort Ossebaar for his guidance during my stay at NIOZ and for the HPLC-MS measurements.

Last, but not least, I would like to thank Timme Donders and Johan Weijers. Timme and Johan together supervised this project and edited the current report and the poster presented at NAC10.
Timme was my mentor during the work done at TNO B&O. He also helped me to collect the samples, used for organic geochemistry, from the core storage of Wintershall B.V. in Beverwijk and provided me with crucial literature and other relevant information.
Johan was my mentor during the work done at Utrecht University, from the start of the lab work in august 2009 till the last sentence of this report in august 2010. Johan served as my soundboard throughout the project. With his enthusiasm for science he opened my ‘scientific eyes’, partly leading to my decision to opt for a PhD position.

Thanks all, bedankt allemaal!

References

Barrett, P. J., (1996). Antarctic paleoenvironment through Cenozoic times—a review. *Terr. Antarct.* 3, 103–119.

Bijlsma, S., (1981). Fluvial sedimentation from the Fennoscandian area into the northwest European Basin during the Late Cenozoic. *Geologie en Mijnbouw* 60, 337–345.

Birks, H.J.B., Birks, H.H., (1980). Quaternary Palaeoecology. Edward Arnold, London. 289 pp.

Brinkhuis, H.,(1994). Late Eocene to early Oligocene dino!agellate cysts from the Priabonian type-area (Northeast Italy); biostratigraphy and palaeoenvironmental interpretation. *Palaeogeogr., Palaeoclimatol., Palaeoecol.* 107, 121–163.

Burger, A.W., (2002). Heavy minerals in the Nieder Ochtenhausen borehole. In: Meyer, K.-J. (Ed.), Forschungsbohrung Nieder Ochtenhausen. Ein Beitrag zur Miozän-Stratigraphie in *NW Deutschland Geologisches Jahrbuch A*, vol. 152, pp. 141–158.

Cameron, T.D.J., Bulat, J., Mesdag, C., (1993). High resolution seismic profile through a Late Cenozoic delta complex in the southern North Sea. *Marine and Petroleum Geology* 10, 591–599.

Clark, P.U., Alley, R.B., Pollard, D., (1999). Northern Hemisphere ice-sheet influences on global climate change. *Science* 286, 1104–1111.

Clausen, O.R., Gregersen, U., Michelsen, O., Sorensen, J.C., (1999). Factors controlling the Cenozoic sequence development in the eastern parts of the North Sea. *Journal of The Geological Society*, London 156, 809–816.

Cortijo, E., Labeyrie, L.D., Elliot, M., Balbon, E., Tisnerat, N., (2000). Rapid climatic variability of the North Atlantic Ocean and global climate: a focus of the IMAGES program. *Quat. Sci. Rev.* 19, 227-241.

Cranwell, P.A., (1973). Chain-length distribution of n-alkanes from lake sediments in relation to post-glacial environmental change. *Freshwater Biology* 3, 259–265.

DeConto, R.M. and Pollard, D., (2003). Rapid Cenozoic glaciation of Antarctica induced by declining atmospheric CO2, *Nature* 421, 245-249.

Donders, T.H., Kloosterboer-van Hoeve, M.L., Westerhoff, W., Verreussel, R.M.C.H., Lotter, A.F., (2007). Late Neogene continental stages in NW Europe revisited. *Earth Sci Rev* 85 (3–4), 161–186.

Donders, T.H., Weijers, J.W.H., Munsterman, D.K., Kloosterboer-van Hoeve, M.L., Buckles, L.K., Pancost, R.D., Schouten, S., Sinninghe Damsté, J.S., Brinkhuis, H., (2009a). Strong climate coupling of terrestrial and marine environments in the Miocene of northwest Europe. *Earth and Planetary Science Letters*, No. 281, 215-225

Donders, T.H., Koolmees, H.H., Bunnik, F.P.M., (2009b), High-resolution pollen analyses of cores A15-03 and A15-04 (southern North Sea) across MIS 94-102. *TNO report TNO-034-UT-2009-01727*, 12 pp.

Etourneau, J., Schneider, R., Blanz, T., Martinez, P., (2010). Intensification of the Walker and Hadley atmospheric circulations during the Pliocene–Pleistocene climate transition. *Earth and Planetary Science Letters*, in press.

Evans, D., Graham, C., Armour, A., Bathurst, P., (2003). The Millenium Atlas: Petroleum Geology of the Central and Northern North Sea. The Geological Society of London. 389 pp.

Farjon, A. (2005). Monograph of Cupressaceae and Sciadopitys. *Royal Botanic Gardens*, Kew, 648 pp.

Fensome, R.A., Williams, G.L., (2004). The Lentin and Williams index of fossil dinoflagellates, 2004 Edition. *AASP Contributions Series*, vol. 42. American Association of Stratigraphic Palynologists Foundation. 909 pp.

Fleet, A.J., Boldey, S.A.R., (Eds.), (1999). Petroleum Geology of Northwest Europe: Proceedings of the 5th Conference. *The Geological Society*, London. Alden Press, Oxford. 1383 pp.

Flower, B.P., Kennett, J.P., (1994). The middle Miocene climatic transition: East Antarctic ice sheet development, deep ocean circulation and global carbon cycling. *Palaeogeogr.*, *Palaeoclimatol.*, *Palaeoecol.* 108, 537–555.

Funnel, B., (1996). Global sea-level and the (pen-)insularity of late Cenozoic Britain. In: Preece, R.C. (Ed.), Island Britain: a Quaternary Perspective. *Geol. Soc. Spec. Pub.*, 96, pp. 3–13.

Gibbard, P.L., West, R.G., Zagwijn, W.H., Balson, P.S., Burger, A.W., Funnel, B.M., Jeffery, D.H., de Jong, J., van Kolfschoten, T., Loster, A.M., Meijer, T., Norton, P.E.P., Treece, R.C., Rose, J., Stuart, A.J., Whiteman, C.A., Zalasiewicz, J.A., (1991). Early and Early Middle Pleistocene correlations in the southern North Sea Basin. *Quaternary Science Reviews* 10, 23–52.

Holbourn, A., Kuhnt, W., Schulz, M., Erlenkeuser, H., (2005). Impacts of orbital forcing and atmospheric carbon dioxide on Miocene ice-sheet expansion. *Nature* 438 (7067), 483.

Glennie, K.W., (1990). Introduction to the Petroleum Geology of the North Sea. Blackwell, Oxford. 402 pp.

Hay, W., (1992). The cause of the late Cenozoic Northern Hemisphere Glaciations: a climate change enigma. *Terra Nova* 4, 305-311

Hedges, J.I., Prahl, F.G., (1993). Early diagenesis: consequences for applications of molecular biomarkers. In: Engel, M.H., Macko, S.A. (Eds.), *Organic Geochemistry: principles and applications.* Plenum Press, New York, pp. 237–253.

Hooghiemstra, H.,(1988). Palynological records from Northwest African marine sediments: a general outline of the interpretation of the pollen signal. *Philos. Trans. R. Soc. Lond., Series B Biol. Sci*. 318 (1191), 431–449.

Hopmans, E.C., Schouten, S., Pancost, R.D., Van der Meer, M.T.J., Sinninghe Damsté, J.S., (2000). Analysis of intact tetraether lipids in archaeal cell material and sediments by high performance liquid chromatography/atmospheric pressure chemical ionization mass spectrometry. *Rapid Commun. Mass Spectrom*. 14, 585–589.

Hopmans, E.C.,Weijers, J.W.H., Schefuß, E., Herfort, L., Sinninghe Damsté, J.S., Schouten, S., (2004). A novel proxy for terrestrial organic matter in sediments based on branched and isoprenoid tetraether lipids. *Earth Planet. Sci. Lett.* 224, 107–116.

Huber, M., Sloan, L.C., (2001). Heat transport, deep waters and thermal gradients: cpoupled simulation of Eocene Greenhouse Climate. *Geophys. Res. Lett*. 28, 3481–3484.

Huuse, M., (2002). Late Cenozoic palaeogeography of the eastern North Sea Basin: climate vs. tectonic forcing of basin margin uplift and deltaic progradation. *Bulletin of the Geological Society of Denmark* 49, 145–170.

Huuse, M., Clausen, O.R., (2001). Morphology and origin of major Cenozoic sequence boundaries in the eastern North Sea Basin: top Eocene, near-top Oligocene and the mid-Miocene unconformity. *Basin Research* 13, 17–41.

Huuse, M., Lykke-Andersen, H., Michelsen, O., (2001). Cenozoic evolution of the eastern North Sea Basin — new evidence from high-resolution and conventional seismic data. *Marine Geology* 177, 243–269.

Jeng, W.L., (2006). Higher plant n-alkane average chain length as an indicator of petrogenic hydrocarbon contamination in marine sediments. *Marine Chemistry* 102, 242–251.

Kemna, H.A., Westerhoff, W.E., (2007). Remarks on the palynology-based chronostratigraphic subdivision of the Pliocene terrestrial deposits in NW-Europe. *Quat. Int.* 164–165, 184–196.

Kennicutt II, M.C., Barker, C., Brooks, J.M.,DeFreitas,D.A., Zhu,G.H., (1987). Selected organic matter source indicators in the Orinoco, Nile and Changjiang deltas. *Organic Geochemistry* 11, 41–51.

Kim, J.-H., Schouten, S., Hopmans, E.C., Donner, B., Sinninghe Damsté, J.S., (2008). Global sediment core-top calibration of the TEX86 paleothermometer in the ocean. *Geochimica et Cosmochimica Acta* 72, 1154–1173.

KNMI, (1997). Royal Netherlands Meteorological Institute (KNMI), World Climate Information (WKI 2.0), available online at:http://www.knmi.nl/klimatologie/normalen1971-2000/wki.html.

Kolla, V., Coumes, F., 1987. Morphology, internal structure, seismic stratigraphy, and sedimentation on the Indus Fan. *Am. Assoc. Petrol. Geol. Bull.* 71, 650–677.

Kuhlmann, G., (2004). High resolution stratigraphy and paleoenvironmental changes in the southern North Sea during the Neogene — an integrated study of Late Cenozoic marine deposits from the northern part of the Dutch offshore area. Ph.D. thesis, Utrecht University, *Geologica Ultraiectina, Mededelingen van de Faculteit Aardwetenschappen*, No. 245, 205 pp.

Kuhlmann, G., Langereis, C., Munsterman, D., van Leeuwen, R.J., Verreussel, R., Meulenkamp, J., Wong, T., (2006) Chronostratigraphy of Late Neogene sediments in the southern North Sea Basin and paleoenvironmental interpretations. *Palaeogeography, Palaeoclimatology, Palaeoecology* 239, 426–455.

Lear, C. H., Elderfield, H. & Wilson, P. A., (2000). Cenozoic deep-sea temperatures and global ice volumes from Mg/Ca in benthic foraminiferal calcite. *Science* 287, 269–272.

Lisiecki, L. E. and Raymo, M. E. A., (2005). Pliocene-Pleistocene stack of 57 globally distributed benthic d18O records. *Paleoceanography* 20.

Marret, F., Zonneveld, K., (2003). Atlas of modern organic-walled dinoflagellate cyst distribution. *Review of Palaeobotany and Palynology* 125, 1–200.

Maslin, M.A., Li, X.S., Loutre, M.F., Berger, A. (1998). The contribution of orbital forcing to the progressive intensification of Northern Hemisphere glaciation. *Quaternary Science Reviews* 17:411-426

McHargue, T.R., Webb, J.E., (1986). Internal geometry, seismic facies, and petroleum potential of canyons and inner fan channels of the inner Indus Submarine Fan. *Am. Assoc. Petrol. Geol. Bull.* 70, 161–180.

Michelsen, O., Thomsen, E., Danielsen, M., Heilmann-Clausen, C., Jordt, H., Laursen, G-V., (1998). Cenozoic sequence stratigraphy in eastern North Sea. In: Graciansky, C.D., Jaquin, T., Vail, P.R., Farley, M.B. (Eds.), Mesozoic and Cenozoic Sequence Stratigraphy of European Basins. *Soc. Econ. Pal. Min. (SEPM), Spec. Pub.*, pp. 91–118.

Müller, P.J., Kirst, G., Ruhland, G., von Storch, I., Rosell-Méle, A., (1998). Calibration of the alkenone paleotemperature index Uk0 37 based on core-tops from the eastern South Atlantic and the global ocean (60°N–60°S). *Geochim. Cosmochim. Acta* 62, 1757–1772.

Nichols, J.E., Booth, R.K., Jackson, S.T., Pendall, E.G. & Huang, Y., (2006). Paleohydrologic reconstruction based on n-alkane distributions in ombrotrophic peat. *Organic Geochemistry*, 37, 1505-13.

Overeem, I., Weltje, G.J., Bishop-Kay, C., Kroonenberg, S.B., (2001). The Late Cenozoic Eridanos delta system in the southern North Sea Basin: a climate signal in sediment supply? *Basin Research* 13, 293–312.

Parker, J.R., (1993). Petroleum Geology of Northwest Europe: Proceedings of the 4th Conference. *The Geological Society*, London. Alden Press, Oxford. 1527 pp.

Pearson, P.N., Bart, E., van Dongen, B.E., Nicholas, C.J., Pancost, R.D., Schouten, S., Singano, J.M., and Wade, B.S., (2007). Stable warm tropical climate through the Eocene Epoch. *Geology*, v. 35 pp. 211-214.

Peterse, F., Schouten, S., van der Meer, J., van der Meer, M.T.J., Sinninghe Damsté, J.S., (2009). Distribution of branched tetraether lipids in geothermally heated soils: implications for the MBT/CBT temperature proxy. *Organic Geochemistry* 40, 201–205.

Poynter, J.G., Eglinton, G., (1990). Molecular composition of three sediments from hole 717C: The Bengal Fan. In: Cochran, J.R., Stow, D.A.V., et al. (Eds.), *Proceedings of the Ocean Drilling Program Scientific Results*, vol. 116, pp. 155–161.

Prahl F. G. and Wakeham S. G. (1987) Calibration of unsaturation patterns in long-chain ketone compositions for paleotemperature assessment. *Nature* 330**,** 367–369.

Pross, J., Klotz, S., (2002). Palaeotemperature calculations from the Praetiglian/Tiglian (Plio-Pleistocene) pollen record of Lieth, northern Germany: implications for the climatic evolution of NW Europe. *Global Planet. Change* 34, 253–267.

Pross, J., Brinkhuis, H., (2005). Organic-walled dino!agellate cysts as paleoenvironmental indicators in the Paleogene; a synopsis of concepts. *Paläontol. Z.* 79 (1), 53–59.

Raymo, M.E., (1994). The initiation of Northern Hemisphere glaciation, *Annu. Rev. Earth Planet. Sci.* 22, pp. 353–383

Redfield, A.C., (1934). On the proportions of organic derivations in sea water and their relation to the composition of plankton. In *James Johnstone Memorial Volume*. (ed. R.J. Daniel). University Press of Liverpool, pp. 177-192.

Reumer, J.W.F., (1989).Speciation and evolution in the Soricidae (Mammalia: Insectivora) in relation with the paleoclimate. *Revue Suisse de Zoologie*, Vol. 96, no. 1, pp. 81-90. 1989.

Rieley, G., Collier, R.J., Jones, D.M., Eglinton, G., (1991). The biogeochemistry of Ellesmere Lake, U.K.—I: source correlation of leaf wax inputs to the sedimentary lipid record. *Organic Geochemistry* 17, 901–912.

Ruddiman, W.F., (2001). Earth's Climate: Past and Future. W.H. Freeman and Company, New York, 465 pp.

Sørensen, J.C., Gregersen, U., Breiner, M., Michelsen, O., (1997). High frequency sequence stratigraphy of Upper Cenozoic deposits in the central and southeastern North Sea areas. *Marine and Petroleum Geology* 14 (2), 99–123.

Schouten, S., Hopmans, E.C., Pancost, R.D., Sinninghe Damsté, J.S., (2000). Widespread occurrence of structurally diverse tetraether membrane lipids: evidence for the ubiquitous presence of low-temperature relatives of hyperthermophiles. *Proc. Nat. Acad. Sci.* U. S. A. 97, 14421–14426.

Schouten, S., Hopmans, E.C., Schefuß, E., Sinninghe Damsté, J.S., (2002). Distributional variations in marine crenarchaeotal membrane lipids: a new tool for reconstructing ancient sea water temperatures? *Earth Planet. Sci. Lett.* 204 (1–2), 265–274.

Schouten, S., Eldrett, J., Greenwood, D. R., Harding, I., Baas, M., and Damsté, J.S.S. (2008). Onset of long term cooling of Greenland near the Eocene-Oligocene boundary as revealed by branched tetraether lipids. Geology 36:147–150.

Schouten, S., Baas, M., Rijpstra, I., (2008), Laboratory manual of the department of Marine Organic Biogeochemistry at the Royal Nethelands Institute for Sea Research (NIOZ), Version 11.

Seki, O., Foster, G.L., Schmidt, D.N., Mackensen, A., Kawamura, K., Pancost, R.D., (2010). Alkenone and boron-based Pliocene pCO_2 records. *Earth and Planetary Science Letters*, No. 292, 201-211

Severinghaus, J.P., Brook, E.J., (1999). Abrupt climate change at the end of the last glacial period inferred from trapped air in polar ice. *Science* 286, 930–934.

Sluijs, A., Pross, J., Brinkhuis, H., (2005). From greenhouse to icehouse; organic walled dinoflagellate cysts as paleoenvironmental indicators in the Paleogene. *Earth Sci Rev* 68, 281–315.

Sluijs, A., Schouten, S., Pagani, M., Woltering, M., Brinkhuis, H., Sinninghe Damsté, J.S., Dickens, G.R., Huber, M., Reichart, G.J., Stein, R., Matthiessen, J., Lourens, L.J., Pedentchouk, N., Backman, J., Moran, K., (2006). Subtropical Arctic Ocean temperatures during the Palaeocene/Eocene thermal maximum. *Nature* 441, 610-613.

Sosdian, S. and Rosenthal, Y., (2009). Deep-Sea Temperature and Ice Volume Changes Across the Pliocene-Pleistocene Climate Transitions. *Science* 325, 306-310

Svenning, J.-C., (2003). Deterministic Plio-Pleistocene extinctions in the European cool-temperate tree flora. *Ecology Letters*, 6, 646–653.

Toney, J.L., Huang, Y., Fritz, S.C., Baker, P.A., Grimm, E., Nyren, P., (2010). Climatic and environmental controls on the occurrence and distributions of long chain alkenones in lakes of the interior United States. *Geochim. Cosmochim. Acta* 74, 1563–1578.

Uda, I., Sugai, A., Itoh, Y.H., Itoh, T., (2001). Variation in molecular species of polar lipids from Thermoplasma acidophilum depends on growth temperature. *Lipids* 36, 103-105.

Van den Brink, F.W.B., de Leeuw, J.P.H.M., van der Velde, G., Verheggen G.M., (1993). Impact of hydrology on the chemistry and phytoplankton development in floodplain lakes along the Lower Rhine and Meuse. *Biogeochemistry* 19: 103-128.

Versteegh, G.J.M., Zonneveld, K.A.F., (1994). Determination of (palaeo) ecological preferences of dinoflagellates by applying detrended and canonical correspondence analysis to late Pliocene dinoflagellate cyst assemblages of the south Italian Singha section. *Rev. Palaeobot. Palynol.* 84, 181–199.

Vinken, (1988). The North West European Tertiary Basins. Results of the international geological correlation programme, project no. 124. *Geologisches Jahrbuch* 100 (508 pp.).

Volkman J.K., Barrett S.M., Blackburn S.I., and Sikes E.L., (1995). Alkenones in *Gephyrocapsa oceanica*: Implications for studies of paleoclimate. *Geochim. Cosmochim. Acta* 59, 513–520.

Weijers, J.W.H., Schouten, S., Hopmans, E.C., Geenevasen, J.A.J., David, O.R.P., Coleman, J.M.,Pancost, R.D., Sinninghe Damsté, J.S., (2006a). Membrane lipids ofmesophilic anaerobic bacteria thriving in peats have typical archaeal traits. *Environ. Microbiol.* 8, 648–657.

Weijers, J.W.H., Schouten, S., Spaargaren, O.C., Sinninghe Damsté, J.S., (2006b). Occurrence and distribution of tetraether membrane lipids in soils: implications for the use of the TEX86 proxy and the BIT index. *Org. Geochem*. 37, 1680–1693.

Weijers, J.W.H., Schouten, S., Van den Donker, J.C., Hopmans, E.C., Sinninghe Damsté, J.S., (2007). Environmental controls on bacterial tetraether membrane lipid distribution in soils. *Geochim. Cosmochim. Acta* 71, 703–713.

Weijers, J.W.H., Schefuß, E., Schouten, S., Sinninghe Damsté, J.S., (2007a). Coupled thermal and hydrological evolution of tropical Africa over the last deglaciation. *Science* 315, 1701–1704.

Weijers, J.W.H., Schouten, S., Sluijs, A., Brinkhuis, H., and Sinninghe Damsté, J.S., (2007b). Warm Arctic continents during the Paleocene-Eocene thermal maximum. *Earth and Planetary Science Letters*, v. 261, 230–238

Weijers, J.W.H. (2007), "Soil-derived branched tetraether membrane lipids in marine sediments: reconstruction of past continental climate and soil organic matter fluxes to the ocean. Ph.D. thesis, Utrecht University, *Geologica Ultraiectina, Mededelingen van de Faculteit Aardwetenschappen*, No. 275, 208 pp.

Welkenhuysen, K. (2006). Het begin van de ijstijden op het noordelijk halfrond in het Gelasiaan (Boven-Plioceen). MSc thesis, Departement Geografie-Geologie, Universiteit Leuven, 77 pp.

Westerhoff, W.E. (2009). Stratigraphy and sedimentary evolution. The lower Rhine-Meuse system during the Late Pliocene and Early Pleistocene (southern North Sea Basin). Ph.D. thesis, Vrije Universiteit Amsterdam, *Geology of the Netherlands* 2, 168 pp.

Whitehead, D.R., (1983). Wind pollination: some ecological and evolutionary perspectives. In: Real, L. (Ed.), *Pollination Biology*. Academic Press, Orlando, pp. 97–108.

Wood, G.D., Gabriel, A.M., Lawson, J.C., 1996. Palynological techniques — processing and microscopy. In: Jansonius, J., McGregor, D.C. (Eds.), *Palynology: principles and applications*. AASP, Salt Lake City, pp. 29–50.

Zachos, J., Pagani, M., Sloan, L., Thomas, E., Billups, K., (2001). Trends, rhythms, and aberrations in global climate 65 Ma to present. *Science* 292, 686–693.

Zachos, J.C., Dickens, G.R., Zeebe, R.E., (2008). An early Cenozoic perspective on green-house warming and carbon-cycle dynamics. *Nature* 451 (7176), 279–283.

Zachos, J. C., Quinn, T. M. & Salamy, K. A., (1996). High-resolution (104 years) deep-sea foraminiferal stable isotope records of the Eocene–Oligocene climate transition. *Paleoceanography* 11, 251–266.

Zagwijn, W.H., (1974b). The Pliocene–Pleistocene boundary in western and southern Europe. *Boreas* 3, 75–97.

Zagwijn, W.H., (1989). The Netherlands during the Tertiary and the Quarternary: a case history of coastal lowland evolution. *Geologie en Mijnbouw* 68, 107–120.

Zhao, M., Rosell, A., Eglinton, G., (1993). Comparison of two UK'37 sea surface temperature records for the last climatic cycle at ODP site 658 from the sub-tropical Northeast Atlantic. *Palaeogeography, Palaeoclimatology and Palaeoecology* 103, 57-65.

Ziegler, (1990). Geological Atlas of Western and Central Europe. 3rd edition. Shell International Petroleum Maatschappij B.V. 239 pp.

Websites

- www.nlog.nl
- www.foraminifera.eu

Appendix 1: Geological time scale

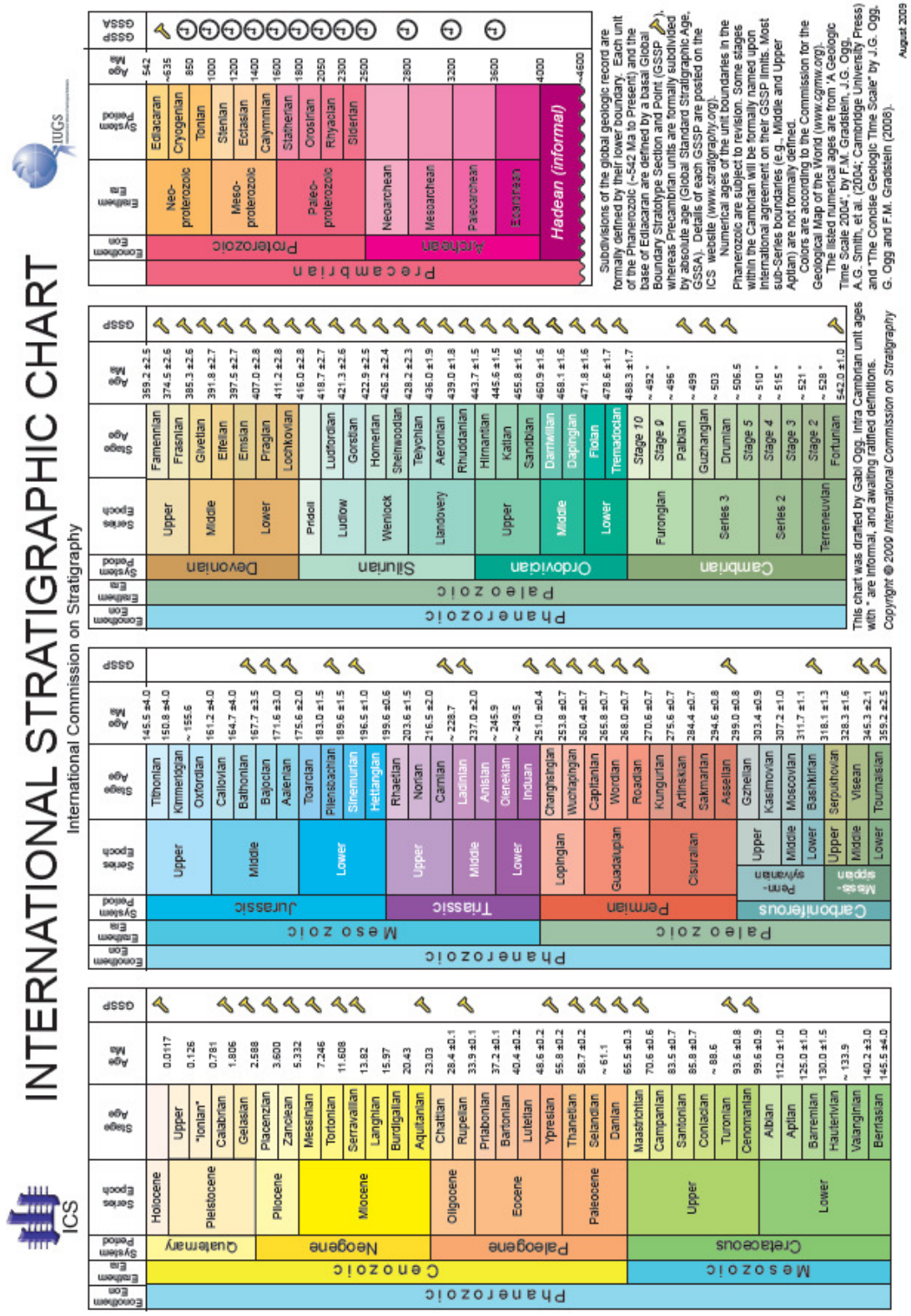

Appendix 2: Studied samples

2.1 Samples used to study the palynology

Core A15-3

Nr.	TNO label	Depth (mbsl)	Nr.	TNO label	Depth (mbsl)
1	CU	400	**62**	**61 CO**	**926.55**
2	CU	445	**63**	**62 CO**	**926.7**
3	CU	450	**64**	**63 CO**	**927.76**
4	CU	470	**65**	**65 CO**	**928.45**
5	CU	490	66	CO	928.5
6	CU	510	**67**	**66 CO**	**929.2**
7	CU	530	**68**	**67 CO**	**929.95**
8	CU	550	**69**	**68 CO**	**935.9**
9	CU	570	**70**	**69 CO**	**936.9**
10	CO	575.42	**71**	**72 CO**	**938.9**
11	CO	594.55	**72**	**73 CO**	**939.8**
12	CU	600	**73**	**75 CO**	**940.9**
13	CO	619.35	74	78 CO	941.9
14	CO	628.6	**75**	**77 CO**	**942.9**
15	CU	650	**76**	**79 CO**	**943.85**
16	CU	670	77	CO	944.4
17	CU	690	**78**	**80 CO**	**944.9**
18	CU	700	**79**	**81 CO**	**945.9**
19	CU	720	**80**	**82 CO**	**946.8**
20	CU	750	**81**	**85 CO**	**946.91**
21	CU	770	**82**	**84 CO**	**947.74**
22	CU	790	83	91 CO	953.25
23	CU	810	**84**	**87 CO**	**954.15**
24	SC	814	**85**	**95 CO**	**955.2**
25	CU	830	86	CO	955.6
26	SC	838	**87**	**89 CO**	**956.18**
27	CU	850	**88**	**90 CO**	**956.31**
28	CU	870	**89**	**92 CO**	**957.3**
29	1 CO	890.05	**90**	**93 CO**	**957.34**
30	CO	890.8	**91**	**94 CO**	**958.25**
31	5 CO	891.75	92	102 CO	959.2
32	3 CO	892.8	**93**	**97 CO**	**960.33**
33	8 CO	893.8	**94**	**98 CO**	**960.67**
34	6 CO	894.8	**95**	**100 CO**	**961.4**
35	11 CO	895.8	**96**	**101 CO**	**962.2**
36	12 CO	896.8	**97**	**103 CO**	**963.17**
37	10 CO	897.8	**98**	**104 CO**	**964.02**
38	15 CO	898.8	**99**	**105 CO**	**964.14**
39	16 CO	899.35	100	CU	975
40	13 CO	899.8	101	CU	985
41	18 CO	900.8	102	CU	990
42	20 CO	901.8	103	CO	995
43	21 CO	902.8	104	CU	1015
44	19 CO	903.85	105	CU	1030
45	CO	904.43	106	CU	1050
46	24 CO	904.8	107	CU	1070
47	25 CO	904.8	108	SC	1079

48	22 CO	905.26	109	SC	1088
49	CO	908	110	CU	1090
50	**48 CO**	**917.55**	111	SC	1100
51	**49 CO**	**918.15**	112	CU	1110
52	**51 CO**	**920**	113	CU	1130
53	52 CO	920	114	CU	1150
54	CO	920.6	115	CU	1170
55	53 CO	920.95	116	CU	1190
56	**54 CO**	**921.05**	117	CU	1210
57	**55 CO**	**921.95**	118	CU	1230
58	**56 CO**	**923**	119	CU	1280
59	**57 CO**	**924**	120	CU	1340
60	**58 CO**	**924.5**	121	CU	1400
61	**60 CO**	**925**			

Note: The palynological samples were collected during different sample-rounds. One sample-round used the core-shift depths, the other rounds the original well-depths. Therefore some depths were sampled double (e.g. 904.8 and 920 mbsl). All depths in this report are based on the core-shift depths.

Core A15-4

Nr.	TNO label	Depth (mbsl)	Splice depth (mbsl) to core A15-3
1	CO	918.4	901.724
2	CO	921.95	904.784
3	27 CO	923.73	906.319
4	28 CO	924.1	906.6
5	29 CO	924.45	906.94
6	30 CO	924.75	907.2
7	31 CO	925.1	907.5
8	32 CO	925.45	907.8
9	34 CO	926	908.276
10	35 CO	926.45	908.65
11	36 CO	926.8	908.966
12	37 CO	927	909.05
13	38 CO	927.45	909.526
14	39 CO	927.8	909.82
15	**40 CO**	**928**	**910.005**
16	**42 CO**	**928.75**	**911.061**
17	CO	929.5	912.143
18	**44 CO**	**929.55**	**912.188**
19	**45 CO**	**930.25**	**913.214**
20	CO	938.1	923.1
21	CO	943.6	928.6
22	116 CO	971.4	956.4
23	CO	974.85	959.85
24	**126 CO**	**975.1**	**960.1**
25	**129 CO**	**976.1**	**961.1**
26	**131 CO**	**976.8**	**961.8**
27	133 CO	977.45	962.45
28	**136 CO**	**978.3**	**963.3**
29	137 CO	978.85	963.85
30	**143 CO**	**980.8**	**965.8**
31	146 CO	981.8	966.8
32	**151 CO**	**983.5**	**968.5**

33	**154 CO**	**984.5**	**969.5**
34	CO	984.8	969.8
35	**158 CO**	**986.15**	**971.064**
36	161 CO	987.15	972
37	165 CO	988.5	973.256
38	**166 CO**	**989**	**973.716**
39	SC	997.8	981.907
40	SC	999.8	983.767
41	SC	1003.8	987.488
42	SC	1008.35	991.721
43	SC	1011.3	994.465
44	SC	1014.3	997.256
45	SC	1064	1037.69
46	SC	1067	1040
47	SC	1070	1042.31
48	SC	1073	1044.62
49	SC	1076	1046.92
50	SC	1079	1049.23
51	CO	1082	1051.54
52	CO	1084	1053.08
53	CO	1085	1053.85
54	CO	1086	1054.62
55	CO	1088	1056.15
56	CO	1089.9	1057.62

Bold = new data counted and added by me

CO = Core (borehole) sample
SC = Side-wall core
CU = Cutting sample

2.2 Samples used for organic geochemistry

Nr.	TNO label	Core	Depth (mbsl)	Splice depth (mbsl) to core A15-3	Box
1	1 CO	A15-3	890.8	890.8	
2	2 CO	A15-3	891.75	891.75	
3	6 CO	A15-3	892.8	892.8	
4	8 CO	A15-3	893.8	893.8	
5	12 CO	A15-3	896.8	896.8	
6	13 CO	A15-3	897.8	897.8	
7	15 CO	A15-3	898.8	898.8	
8	17 CO	A15-3	899.8	899.8	6-1
9	20 CO	A15-3	901.8	901.8	6-4
10	23 CO	A15-3	903.85	903.85	6-6
11	24 CO	A15-3	904.8	904.8	6-7
12	32 CO	A15-4	925.45	907.8	
13	36 CO	A15-4	926.8	908.97	
14	38 CO	A15-4	927.45	909.53	
15	40 CO	A15-4	928	910.01	
16	42 CO	A15-4	928.75	911.06	
17	44 CO	A15-4	929.55	912.19	
18	45 CO	A15-4	930.25	913.21	
19	48 CO	A15-3	917.55	917.55	8-1
20	49 CO	A15-3	918.15	918.15	8-2
21	51 CO	A15-3	920	920	8-4
22	55 CO	A15-3	921.95	921.95	8-6
23	57 CO	A15-3	924	924	8-8
24	60 CO	A15-3	925	925	8-10
25	62 CO	A15-3	926.7	926.7	9-1
26	67 CO	A15-3	929.95	929.95	9-5
27	68 CO	A15-3	935.9	935.9	10-2
28	69 CO	A15-3	936.9	936.9	10-3
29	72 CO	A15-3	938.9	938.9	10-5
30	75 CO	A15-3	940.9	940.9	10-7
31	77 CO	A15-3	942.9	942.9	10-9
32	79 CO	A15-3	943.85	943.85	10-10
33	80 CO	A15-3	944.9	944.9	11-1
34	81 CO	A15-3	945.9	945.9	11-2
35	85 CO	A15-3	946.91	946.91	11-3
36	86 CO	A15-3	953.25	953.25	12-1
37	87 CO	A15-3	954.15	954.15	12-2
38	89 CO	A15-3	956.18	956.18	12-4
39	92 CO	A15-3	957.3	957.3	12-5
40	94 CO	A15-3	958.25	958.25	12-6
41	97 CO	A15-3	960.33	960.33	12-9
42	101 CO	A15-3	962.2	962.2	13-1
43	103 CO	A15-3	963.17	963.17	13-2
44	104 CO	A15-3	964.02	964.02	13-3
45	126 CO	A15-4	975.1	960.1	
46	129 CO	A15-4	976.1	961.1	
47	131 CO	A15-4	976.8	961.8	
48	133 CO	A15-4	977.45	962.45	
49	136 CO	A15-4	978.3	963.3	

50	137 CO	A15-4	978.85	963.85	
51	143 CO	A15-4	980.8	965.8	
52	146 CO	A15-4	981.8	966.8	
53	151 CO	A15-4	983.5	968.5	
54	154 CO	A15-4	984.5	969.5	
55	158 CO	A15-4	986.15	971.06	
56	161 CO	A15-4	987.15	972	
57	CO	A15-4	997.8	981.91	
58	CO	A15-4	999.8	983.77	
59	CO	A15-4	1003.8	987.49	
60	CO	A15-4	1008.35	991.72	
61	CO	A15-4	1011.3	994.47	
62	CO	A15-4	1014.3	997.26	
63	SC	A15-4	937.8	922.8	
64	SC	A15-4	938.45	923.45	
65	SC	A15-4	1008.05	991.44	
66	SC	A15-4	1008.75	992.09	
67	SC	A15-4	1064	1037.69	
68	SC	A15-4	1067	1040	
69	SC	A15-4	1070	1042.31	
70	SC	A15-4	1073	1044.62	
71	SC	A15-4	1076	1046.92	
72	SC	A15-4	1079	1049.23	
73	SC	A15-4	1082	1051.54	
74	SC	A15-4	1084	1053.08	
75	SC	A15-4	1085	1053.85	
76	SC	A15-4	1086	1054.62	
77	SC	A15-4	1088	1056.15	
78	SC	A15-4	1089.9	1057.62	

CO = Core (borehole) sample
SC = Side-wall core
CU = Cutting sample

Note: A15-3 890.8 mbsl and A15-3 898.8 mbsl were extracted both with ASE and ultrasonically. A15-3 953.25 mbsl was extracted two times. No TOC-data available for A15-4 938.45 mbsl.

2.3 Samples used for isotope analysis

Sample Nr.	Core	Depth (mbsl)	Splice to A15-3	Sample Nr.	Core	Depth (mbsl)	Splice to A15-3
4	A15-3	893	893	114	A15-4	970,82	955,82
5	A15-3	893,95	893,95	115	A15-4	971	956
6	A15-3	894,8	894,8	116	A15-4	971,4	956,4
10	A15-3	897,8	897,8	117	A15-4	971,8	956,8
14	A15-3	900	900	118	A15-4	972,1	957,1
15	A15-3	901	901	119	A15-4	972,45	957,45
16	A15-3	901,55	901,55	121	A15-4	973,1	958,1
17	A15-3	902	902	122	A15-4	973,45	958,45
18	A15-3	903	903	123	A15-4	973,75	958,75
19	A15-3	903,85	903,85	124	A15-4	974,05	959,05
20	A15-3	904	904	125	A15-4	974,45	959,45
21	A15-3	905	905	127	A15-4	975,45	960,45
22	A15-3	905,26	905,26	128	A15-4	975,85	960,85
23	A15-3	906,05	906,05	129	A15-4	976,1	961,1
24	A15-3	907	907	130	A15-4	976,4	961,4
26	A15-3	907,46	907,46	131	A15-4	976,8	961,8
48	A15-3	917,55	917,55	132	A15-4	977,1	962,1
49	A15-3	918,15	918,15	134	A15-4	977,8	962,8
50	A15-3	918,15	918,15	135	A15-4	978,1	963,1
75	A15-3	939	939	136	A15-4	978,3	963,3
86	A15-3	950,05	950,05	137	A15-4	978,85	963,85
90	A15-3	953,11	953,11	139	A15-4	979,45	964,45
93	A15-3	954,14	954,14	140	A15-4	979,8	964,8
97	A15-3	957,13	957,13	141	A15-4	980,2	965,2
100	A15-3	958	958	142	A15-4	980,5	965,5
105	A15-3	960,94	960,94	143	A15-4	980,8	965,8
29	A15-4	924,45	906,94	144	A15-4	981,15	966,15
31	A15-4	925,1	907,5	145	A15-4	981,5	966,5
32	A15-4	925,45	907,8	146	A15-4	981,8	966,8
34	A15-4	926	908,28	147	A15-4	982,15	967,15
35	A15-4	926,45	908,67	149	A15-4	982,8	967,8
36	A15-4	926,8	908,966	151	A15-4	983,5	968,5
37	A15-4	927	909,13	152	A15-4	983,8	968,8
38	A15-4	927,45	909,526	153	A15-4	984,15	969,15
39	A15-4	927,8	909,83	154	A15-4	984,5	969,5
40	A15-4	928	910,005	155	A15-4	985,2	970,18
42	A15-4	928,75	911,061	157	A15-4	985,8	970,75
43	A15-4	928,95	911,33	158	A15-4	986,15	971,064
46	A15-4	930,5	913,6	159	A15-4	986,5	971,4
47	A15-4	931	914,29	160	A15-4	986,8	971,68
108	A15-4	969,25	954,25	161	A15-4	987,15	972
109	A15-4	969,55	954,55	163	A15-4	987,8	972,6
110	A15-4	969,85	954,85	164	A15-4	988,1	972,88
112	A15-4	970,3	955,3	165	A15-4	988,5	973,26
113	A15-4	970,55	955,55	166	A15-4	989	973,72